Virtually Transparent TiO 2 /Polyelectrolyte Thin Multilayer Films as High Efficiency Nanoporous Photocatalytic Coatings for Breaking Down Formic Acid and for E. Coli Removal

Marvin Motay, David Martel, Bertrand Vileno, Charline Soraru, Lydie Ploux,
María Guadalupe Méndez-Medrano, Christophe Colbeau-Justin, Gero Decher,
Nicolas Keller

▶ To cite this version:

Marvin Motay, David Martel, Bertrand Vileno, Charline Soraru, Lydie Ploux, et al.. Virtually Transparent TiO 2 /Polyelectrolyte Thin Multilayer Films as High Efficiency Nanoporous Photocatalytic Coatings for Breaking Down Formic Acid and for E. Coli Removal. ACS Applied Materials & Interfaces, In press. ⟨hal-03046440⟩

HAL Id: hal-03046440
https://hal.science/hal-03046440v1

Submitted on 8 Dec 2020

HAL is a multi-disciplinary open access archive for the deposit and dissemination of scientific research documents, whether they are published or not. The documents may come from teaching and research institutions in France or abroad, or from public or private research centers.

L'archive ouverte pluridisciplinaire **HAL**, est destinée au dépôt et à la diffusion de documents scientifiques de niveau recherche, publiés ou non, émanant des établissements d'enseignement et de recherche français ou étrangers, des laboratoires publics ou privés.

Autorisation HAL

HAL Authorization

Virtually Transparent TiO_2/Polyelectrolyte Thin Multilayer Films as High Efficiency Nanoporous Photocatalytic Coatings for Breaking Down Formic Acid and for E. Coli Removal

Marvin Motay,[a,b] *David Martel,*[b] *Bertrand Vileno,*[c] *Charline Soraru,*[d] *Lydie Ploux,*[d,e] *María Guadalupe Méndez-Medrano,*[f] *Christophe Colbeau-Justin,*[f] *Gero Decher,*[b] *Nicolas Keller*[a,] *

[a] Institut de Chimie et Procédés pour l'Energie, l'Environnement et la Santé (ICPEES), CNRS, Université de Strasbourg, 25 rue Becquerel 67087 Strasbourg, France

[b] Institut Charles Sadron (UPR 22), CNRS, Université de Strasbourg, 23 rue de Loess, 67034, Strasbourg Cedex 2, France

[c] Institut de Chimie, CNRS, Université de Strasbourg, CNRS, 1 rue Blaise Pascal 67008 Strasbourg Cedex, France

[d] Institut de Science des Matériaux de Mulhouse (IS2M, UMR7361 CNRS/Université de Haute Alsace), 15 rue Jean Starcky, 68057 Mulhouse, France

[e] Biomaterial Bioengineering (U1121 INSERM/Université de Strasbourg), 11 rue Humann, 67000 Strasbourg, France

[f] Institut de Chimie, CNRS UMR 8000, Université Paris-Saclay, 91405 Orsay, France

corresponding author: * nkeller@unistra.fr

KEYWORDS. Layer-by-Layer assembled films ; TiO_2 nanoparticles ; photocatalytic coatings; quantum yield ; formic acid mineralization ; antibacterial properties.

ABSTRACT.

Virtually transparent photocatalytic multilayer films composed of TiO_2 nanoparticles and polyelectrolytes were built on model surfaces using layer-by-layer assembly and investigated as photocatalytic nanoporous coatings. Formic acid (HCOOH) and *Escherichia coli* were used as models for the degradation of gaseous pollutants and for studying antibacterial properties. Positively charged TiO_2 nanoparticles were co-assembled with negatively charged poly (sodium 4-styrenesulfonate) (NaPSS) which leads to highly transparent nanoscale coatings in which the content of TiO_2 particles is controlled mainly by the number of deposition cycles and the enhanced translucency with respect to titania powders is likely due to the presence of the polyelectrolytes in the interstitial space between the particles. Build-up and structural properties of the films were determined by ellipsometry, Quartz Crystal Microbalance (QCM-D, with dissipation monitoring), UV-Vis spectrophotometry in transmission and scanning electron microscopy. Complementary photophysical and activity tests of $(PSS/TiO_2)_n$ multilayer films were performed in the gas-phase under UV-A light and revealed a peculiar dependence on the number of layer pairs, corresponding to a clear deviation from the usual observations in photocatalysis with increasing TiO_2 amounts. Most notably, a single layer pair film showed a strongly enhanced HCOOH mineralization and outperformed films with a higher number of layer pairs, with respect to the quantity of TiO_2 catalyst present in the films. It is believed that the high quantum yield (8.1%) of a coating consisting of a single TiO_2 layer which is 6-7 times higher than that of a film consisting of 6-10 layer pairs could be due to the optimum accessibility of the TiO_2 crystallites towards both HCOOH and water molecules. In thicker films, while no detrimental light screening was observed with increasing the number of layer pairs, diffusion

phenomena could cap the efficiency of the access of the pollutant and water to the catalytic surface. Unlike for HCOOH mineralization, three PSS/TiO_2 layer pairs were required for observing a maximum antibacterial activity of the nanocomposite coatings. This is likely due to the fact that micron-size *E.coli* bacteria do not enter into the interstitial space between the TiO_2 particles and require a different surface morphology with respect to the number of active contact points for an optimum degradation.

1. INTRODUCTION

Heterogeneous photocatalysis gained importance in the last decades for facing new challenges and addressing major societal concerns on environment, sustainable chemistry and energy demand.[1,2] Up to now, wide band-gap titanium dioxide (TiO_2) remains the most efficient single-phase photocatalyst when exposed to artificial or natural UV-A light for the implementation of photoactive surfaces or the development of environmental remediation technologies for purifying air or water.[3,4,5,6] Therefore, the immobilization of TiO_2 in thin photocatalytic coatings found growing attention, either for elaborating self-cleaning surfaces or for being stabilized into photocatalytic reactors.[7,8,9] Among many bottom-up-type methods such as e.g. sol-gel synthesis or chemical/physical vapor deposition, the self-assembly approach in which molecules and/or particles assemble themselves without the presence of outside interactions, is very promising.[10]

Layer-by-Layer (LbL) is a scalable technology for building high-quality solution-processed nano-composite films from a large choice of different components.[11,12,13] This versatile technique enables the development of function-specific multilayer assemblies for providing new or complementary properties to substrates, through the alternate deposition of oppositely-charged materials on charged surfaces. First applied for preparing polyelectrolyte multilayers, LbL assembly is a simple yet powerful process for preparing multi-material films with tunable properties, and has consequently been extended to many other charged components for building sandwich-like superstructures.[14,15,16,17,18]

LbL assembly has the advantage that it can be applied on model surfaces for a controlled monitoring of for example film growth or for a more detailed understanding of the film properties. In addition it can also be used for forming highly similar coatings at identical deposition conditions on more complex, irregular surfaces that suffer from a lack of characterization methods. This way the deposition can be optimized using structural data from model surfaces (for example quartz slides or Si-wafers) while the performance data of a nano-composite material are obtained from application-relevant substrates (for example textiles). Another advantage arises from the fact that the "soft" self-assembly conditions allow for preparing stable photocatalytic coatings on mechanically fragile or thermally sensitive surfaces.

The past years have brought an increasing number of applications of the LbL self-assembly method in a large variety of fields, among which the photocatalytic applications are an especially fast-developing area as multilayer films are often transparent, whether environmental remediation, self-cleaning/decontaminating or hydrogen production applications are concerned.[13,19,20,21,22,23,24,25,26,27] Further, the amphoteric properties of most of the photocatalytic materials (eg. titania) favors its versatile incorporation within multilayer films, by allowing negatively or positively-charged titania suspensions to be prepared by suitably adjusting the pH acidic or alkaline media.[13,28]

Some of the recent investigations of photocatalytic LbL films concern the gas phase heterogeneous photocatalytic oxidation for the mineralization of air pollutant such as 2-propanol,[29,30] acetaldehyde,[31] hydrogen sulfide [32] or ammonia,[33] as well as chloroethyl ethyl sulfide as model of chemical warfare agents.[34] The elaboration of antibacterial photocatalytic surfaces has also been studied for developing self-disinfecting textiles.[22]

Here we report on the development of homogeneous, nano-porous and virtually optically transparent LbL thin films containing Aeroxide® TiO_2 P25 nanoparticles - currently the *de-facto* commercial reference photocatalyst [35,36] - with photocatalytic activity under UV-A light in both gas phase degradation of formic acid and *Escherichia coli* (*E. coli*) bacteria inactivation. We demonstrate here the peculiar photocatalytic behavior of the films with regard to the layer number, that deviates from the usual trend observed in photocatalysis with increasing the photocatalyst amount, and we consequently discussed on the high HCOOH mineralization and quantum yields obtained on the film built with only one single layer pair. *E. coli* bacteria was used for assessing the antibacterial efficiency of the films, since this very-well documented bacteria can be identified as causing microbial problems in a variety of contexts. Indeed, many of them are responsible for infections, with detrimental consequences resulting from their population growth, due to either their pathogenicity or the imbalance of a microbiological ecosystem leading to excessive growth of a commensal population. Formic acid (HCOOH) was taken as gas phase model compound for assessing the photocatalytic activity and the behavior of the multilayer films towards gaseous chemical pollution, although it is not considered as one of the main encountered Volatile Organic Compounds (VOCs). Indeed, HCOOH is the main reaction intermediate formed during the photocatalytic oxidation of formaldehyde (one of the most problematic VOCs from indoor air), and the ultimate reaction intermediate observed in the photocatalytic degradation of many VOCs like acetone or 2-butanone. Also, formic acid can be directly mineralised into water and carbon dioxide without the formation of any long-lived gaseous intermediates.[5,37] In addition, HCOOH by-itself can give rise to irritation and tissues and organs with high oxygen consumption are vulnerable to HCOOH exposures.[38]

2. EXPERIMENTAL

2.1 Materials and substrates

Aeroxide® titanium dioxide (TiO_2) P25 was provided by Evonik (Germany) as a fine powder. Poly(ethyleneimine) (PEI, $M_w \approx 750\,000$ g/mol, 50 wt. % in water), Poly(sodium 4-styrenesulfonate) (PSS, Mw ≈ 70 000 g/mol) and Poly(diallyldimethyliammonium chloride) (PDDA, Mw ≈ 100 000 – 200 000 g/mol, 20 wt.% in water) were purchased from Sigma Aldrich.

Nitric acid (HNO_3) 68% and Formic acid (HCOOH, reagent grade >95%) were bought from Prolabo and Sigma-Aldrich, respectively. Milli-Q water (ultrapure water) with a resistivity of 18.2 MΩ.cm was obtained from a Milli-Q gradient (Millipore, France) at 25°C. Hellmanex III (Hellma Analytics) was purchased from Sigma Aldrich. Ethanol (99.5% absolute anhydrous) was bought from Carlo Erba.

Silicon wafers with an orientation of <100> were purchased from WaferNet INC (San José, CA, USA). Glass (microscope) slides were purchased from Roth (Germany). 1 mm thickness quartz slides (Suprasil) were purchased from Thuet B. France (Blodelsheim, France). Gold coated quartz crystals (AT-cut quartz crystals with a 5 MHz fundamental frequency) used for QCM-D characterisations, were purchased from Q-sense – Biolin Scientific (Sweden). The preparation of the different substrates has been described in Supporting Information SI1.

2.2 Preparation of polyelectrolyte solutions and suspensions

Positively-charged poly(ethylene imine) (PEI) solution was prepared at a concentration of 1 $g \cdot L^{-1}$ in Milli-Q water. Negatively-charged poly(sodium 4-styrenesulfonate) (NaPSS) solution was prepared at a concentration of 1 $g \cdot L^{-1}$ in Milli-Q water at pH 2.5 (adjusted by HNO_3).

Since TiO_2 has amphoteric properties due to its surface groups ($TiOH_2^+$ or TiO^- respectively in acidic or alkaline media), negatively or positively-charged suspensions can be prepared by adjusting the pH.[13,28] 2 g of TiO_2 were added to 80 mL Milli-Q water with pH 2.5 (adjusted by HNO_3) and stirred for 1 h. The positively-charged TiO_2 suspension obtained at 25 $g.L^{-1}$ was then sonicated using a tip-sonicator at a 300 W power for 25 min in order to prevent as much aggregation as possible. The suspension was cooled down to room temperature and centrifugated at 3700 rpm for 15 min to collect only the smallest aggregates. The remaining suspension was 12.25 ± 0.21 $g \cdot L^{-1}$ (value obtained by ICP-AES) and had a milky white colour. The pH of the suspensions was checked prior to the film constructions.

2.4 Multilayered thin film construction by Layer-by-Layer deposition

Layer-by-Layer (LbL) assembly was performed by the immersion of substrates (“dipping”) in solutions successively depositing oppositely-charged compounds on the model substrates. Positively-charged PEI was used as an adhesion promotor to facilitate the deposition of the first layer on different substrates, and negatively-charged PSS was further deposited on the PEI layer for acting as a glue between consecutively deposited TiO_2 layers. In order to preserve the TiO_2 positive surface charges, PSS was dissolved in acidic milli-Q water at pH 2.5 adjusted by HNO_3.

Once activated by an oxygen plasma, the silicon wafer substrate (4.5 x 8 cm) is immerged in the positively-charged PEI solution at 1 $g.L^{-1}$ for 20 min and rinsed by three successive 3 min-long immersions in Milli-Q water for 3 min. Due to overcompensation of charges, the substrate surface was positively charged. After being dried by compressed air, the substrate was dipped in the negatively-charged PSS solution for 20 min. The substrate was then rinsed 3 times in acidic Milli-Q water at pH 2.5 for 3 min and dried with compressed air. In the same way as previously stated, the substrate was immersed in the positively-charged TiO_2 suspension, rinsed in acidic Milli-Q water and dried with compressed air. The substrate surface was positively charged and the (PSS/TiO_2) pair of layers was constructed. The PSS and TiO_2 deposition steps were repeated until the desired number of pairs of layers was reached. Films were labelled as $PEI/(PSS/TiO_2)_n$, n being the number of layer pairs deposited.

2.5 Characterization methods

The amount of titanium in the TiO_2 suspensions and in the LbL films was obtained by Inductively Coupled Plasma - Atomic Emission Spectroscopy (ICP-AES). The X-ray diffraction (XRD) patterns of the samples were recorded on a D8 Advance Brucker powder diffractometer in a θ/θ mode using the Cu $K\alpha_1$ radiation at 1.5406 Å.

Top-view Scanning Electron Microscopy (SEM) images were recorded on JEOL JSM-6700 F FEG microscope with an acceleration voltage of 3 kV. Hitachi SU8010 microscope was used for characterising the cross sections of titania and polyelectrolytes LbL films with an acceleration voltage of 10 kV. The films were cut by a cross section polisher IM4000Plus (Hitachi) using Ar beam and acceleration tension of 6 KeV.

Dynamic Light Scattering (DLS) measurements were done on a Zetasizer NanoZS device (Malvern Instrument Ltd, UK) at a scattering angle of 173° and a wavelength of 632.8 nm (He/Ne laser) at 25°C. The analyses were triplicated and the cuvettes were rinsed with Milli-Q water and acidic Milli-Q water (pH 2.5, HNO_3) prior to introduction of the TiO_2 suspension.

Ellipsometry. Ellipsometric measurements of the LbL films were performed using a PLASMOS SD 2300 ellipsometer operating at the single wavelength of 632.8 nm and a constant angle of 70° for monitoring the film construction on silicon wafers and for estimating the film thickness.[39] A constant refractive index of the films equal to that of SiO_2 (1.465) was assumed due to the difficulty of determining the refractive index independently especially with respect to for small layer numbers. Each film thickness was obtained by measuring 10 different point areas randomly selected all along the surface of the Si wafer, and the error bars were the standard deviations of these measurements (including the error bar resulting from each measurement as well), providing indications on the film thickness homogeneity.

Quartz Crystal Microbalance with Dissipation monitoring (QCM-D) measurement. QCM-D measurements were carried out on the LbL films in a QCM-D E4 (Q-Sense AB, Sweden) using flow modules in parallel. In situ LbL assemblies of TiO_2 nanoparticles and polyelectrolytes were done in a similar manner to those on macroscopic silicon or glass/quartz substrates except that for QCM-D, the LbL assembly was done in parallel (detailed protocol in Supporting Information SI2). Upon the excitation of the crystal at the fundamental frequency of 5 MHz, the resonance frequency increase observed at the fundamental as well as the overtone frequencies is associated with the increase in hydrodynamic mass deposited onto the crystal surface during the film assembly through the Sauerbrey equation.[40] Energy dissipation due to viscoelastic film adsorption is reflected by the change in dissipation factor, defined as the ratio between the energy dissipated and stored in the crystal during a single oscillation. In this work, the QCM slide had a proportionality coefficient of 17.7 ng/(cm²•Hz) and calculations were made at the 3rd, 5th and 7th overtone, considering that the observation from the fundamental frequency is usually not used as it tends to be subjected to artifacts from the sensor clamp.[41]

UV-vis spectrophotometry. UV-visible spectrophotometry was performed on LbL films in the transmission mode using quartz slides (2.5 x 4.5 cm) as substrates in a UV-Visible Varian® 100 Scan spectrophotometer. Plasma treatment was applied on both sides of the quartz slide so that polyelectrolytes and titania layers were coated evenly on both sides, and 6 layers of TiO_2 were deposited on each side of the quartz slide before reaching signal saturation in the UV-C region, corresponding to 12 PSS/TiO_2 layer pairs in total. The absorbance measured after each deposition step was therefore divided by two, for obtaining the absorbance increment corresponding to a single layer pair PSS/TiO_2 deposited and globally for measuring the absorbance of the PEI/(PSS/TiO_2)$_n$ films. Supporting Information SI3 shows the methodology used for estimating the mass of catalyst deposited per layer per surface area.

Time Resolved Microwave Conductivity (TRMC). The charge-carrier lifetimes in the LbL films upon UV illumination were determined by microwave absorption experiments using the TRMC method.[42] This technique, already used to characterized TiO_2 based semiconductors,[43,44] is based on the measurement of the change of the microwave power reflected by a sample, induced by its laser pulsed illumination.This relative variation of microwave absorption can be correlated, for small perturbations of conductivity, to the variation of sample conductivity. In the case of TiO_2, the TRMC signal can be attributed to free electrons created in the band gap.

The incident microwaves were generated by a Gunn diode of the K_α band at 30 GHz. Pulsed light source was an OPO laser (EKSPLA, NT342B) tunable from 225 to 2000 nm. It delivers 8 ns fwmh pulses with a frequency of 10 Hz. The light energy density received by the sample was 1.3 mJ cm^{-2} at 350 nm. The main data provided by TRMC are the maximum value of the signal (I_{max}), which indicates the number of the excess charge carriers created by the pulse, including decay processes during the excitation by the laser (10 ns), and the decay ($I(t)$) due to the decrease of the excess electrons, either by recombination or by trapping processes. Concerning the decay, i.e. the lifetime of charge carriers, a short and a long range is usually analysed. The shortrange decay, arbitrarily fixed up to 40 ns after the beginning of the pulse, represented by the I_{40ns}/I_{max} ratio, reflects fast processes, mainly recombination of charge carriers, a high value indicating a low recombination speed. Details can be found in Supporting Information SI4.

Electron Paramagnetic Resonance (EPR). EPR investigations were performed on the LbL films on a continuous-wave EPR X-band spectrometer (EMXplus from Bruker Biospin GmbH, Germany) equipped with a high-sensitivity resonator (4119HS-W1, Bruker). This setup was used to record conventional field-swept spectra of functionalized capillaries filled with aqueous solutions supplemented by spin scavenger molecules (TEMPOL, 4-hydroxy-2,2,6,6-tetramethylpiperidine 1-oxyl, Aldrich). Measurements were performed in short intervals between subsequent irradiation periods of 30 s. The principal experimental parameters values were a modulation amplitude of 0.5 G, a microwave power of 1.8 mW, a time constant of *ca.* 20 ms and a conversion time of *ca.* 50 ms. 120 G were swept in 60 s per scan recorded after each illumination step. The film construction inside the glass capillaries (rincaps 50 μL, ca. 1 mm inner diameter from Hirschmann, Germany) was adapted from the procedure we developed in Twardoch *et al.*,[45] using in that case acidic pH conditions for the TiO_2 nanoparticle suspension, and detailed in SI2. Illumination of the capillaries was performed outside the EPR cavity with an UV neon-based lab-made illumination chamber. Each neon presents a λ_{max} = 365 nm ($h\nu$ = 3.4 eV) and $E \approx 1.5$ mW.cm^{-2}. The emission spectra of the neons and a schematic description of the experimental setup are presented in Supporting Information SI5.

2.5 Gas-phase photocatalytic tests

The photocatalytic activity and behavior of LbL films on model surfaces have been assessed by their ability to degrade and mineralize gaseous HCOOH under UV-A irradiation in a single-pass continuous gas flow reactor, with a flat configuration derived from that detailed in the ISO 22197 standard series (More details on the reactor and on the experimental setup can be found in Supporting Information SI6).[46,47] The reactor was placed in a thermostated chamber for maintaining a constant temperature of 25°C during the test according to ISO standards, since heat generated by the lamp during the irradiation could not be neglected. The photocatalytic tests were performed at a gaseous HCOOH concentration of 45 ppm$_v$, at a relative humidity of 50% (about 3% relative to the total atmospheric pressure), and with a total air flow rate of 20 ml/min, corresponding to a velocity of 0.74 cm/s^{-1} and a residence time of 10.8 s in the reaction zone of the reactor.

The photocatalysts were first exposed to the inlet polluted air flow with no illumination until dark adsorption equilibrium was reached, before the UV-A illumination was switched on. The UV-A illumination was provided by a 8W UV-A blacklight lamp (Sylvania Blacklight Blue F8W/BLB T5), with a spectral peak centered on 365 nm, placed above the reactor (1.5 cm), parallel to the film. The film was exposed to an irradiance of 2.5 mW.cm^{-2}, recorded using a wideband spectroradiometer (RPS900-W ILT). The catalytic activity was evaluated under steady state conditions, typically achieved after 3 h of irradiation. No change in activity was observed for all samples for 24 h after reaching steady state conditions.

The photocatalytic performances were obtained by *on-line* quantifying both inlet and outlet flows using a R3000A gas micro-chromatography (SRA instruments), equipped with thermal conductivity micro-detectors, allowing quantification of HCOOH, water and CO_2. All the photocatalytic tests have been performed twice, and the photocatalytic data corresponded to the averaged data, with a relative accuracy of ± 5%.

The photocatalytic activity of the films was expressed in terms of both HCOOH conversion and CO_2 formed, while the CO_2 concentration was compared to the stoichiometric CO_2 concentration, corresponding to 100% selectivity to CO_2 of the HCOOH oxidation reaction (Eq. 2-3).

$$\text{HCOOH conversion (\%)} = \frac{[\text{HCOOH}_{\text{in}}]-[\text{HCOOH}_{out}]}{[\text{HCOOH}_{\text{in}}]} \times 100 \tag{2}$$

$$\text{Theoretical CO}_2\ (\text{ppm}_\text{v}) = [\text{HCOOH}_{\text{in}}] - [\text{HCOOH}_{\text{out}}] \tag{3}$$

The activity of the photocatalytic films was also expressed in terms of quantum yields, calculated for a wavelength range from 300 to 800 nm. Quantum yields are based on a “number ratio”, either of photoconverted molecules over absorbed photons or over photons entering the reactor.[48]

The apparent quantum yield η_{app}, takes into account the reaction rate and the rate (flux) of photons emitted by the UV-A lamp (and more precisely the rate of photons received by the film), while the efficient quantum yield (or quantum yield) η takes into account the number of photons that have been absorbed by the films, as follows:

$$\eta_{\text{app}} = \frac{\text{r}}{\phi_{\text{received}}} \tag{4}$$

$$\eta = \frac{\text{r}}{\phi_{\text{absorbed}}} \tag{5}$$

where r is the reaction rate (in mol of HCOOH/min), $\phi_{received}$ is the rate of received photons and $\phi_{absorbed}$ is the rate of photons absorbed with :

$$\Phi_{\text{received}} = \int_{\lambda_{min}}^{\lambda_{max}} \frac{P(\lambda)}{E(\lambda)}\, d(\lambda) \tag{6}$$

$$\Phi_{\text{absorbed}} = \int_{\lambda_{min}}^{\lambda_{max}} \frac{P(\lambda) \times (1 - 10^{-A(\lambda)})}{E(\lambda)}\, d(\lambda) \tag{7}$$

P is the irradiation power at a given wavelength (in W) with $P(\lambda) = I(\lambda) \times 10^{-6} \times S$ with I being the irradiance received by the film surface (W.cm^{-2}) and S the surface area of the film (36 cm^2). E is the photon energy (in J) with $\text{E} = \frac{\text{hc}}{\lambda}$.

2.6 Photocatalytic antibacterial activity of the substrates

Experiments were conducted with a GFP-producing *E. coli* strain, *E. coli* SCC1.[49,50] −80°C frozen bacterial cells were spread on a LB (Lysogeny broth, Sigma-Aldrich) agar plate and cultured at 30°C for 48 h. A first suspension was prepared with one colony in LB, incubated overnight at 30°C and used to prepare a second suspension (10% vol. in fresh LB). After incubation for 4 h at 30°C, bacteria were harvested by centrifugation and re-suspended in physiological serum (NaCl (9 g/L, pH 6.8) adjusted to a 600 nm absorbance of 0.1 ($5\ 10^7$ CFU mL^{-1}). The material substrates were placed in 35 mm Petri dishes and inoculated with 3 ml of this suspension. After 3 h of incubation at 30°C, they were washed three times with 2 ml physiological serum without creating air-surface interface. Adhered bacteria were *in situ* observed (i.e., in the last washing solution) under a fluorescence confocal microscope (LSM700, Carl ZEISS) equipped with a X63 water immersion objective (W Plan Apochromat X63/1.0, 2.0 mm) (excitation and acquisition wavelengths at 488 nm and 528 nm respectively). The substrates were exposed to UV-A irradiation (3 mW/cm^2) for 60 min and propidium iodide (PI, Aldrich-Sigma) dye was added to stain membrane-damaged bacteria. Again, adhered bacteria were *in situ* observed under the confocal microscope (excitation and acquisition wavelengths at 488 nm and 645 nm respectively). For biofilm assessment, the last washing solution was replaced by LB medium for 15 h of further growth at 30°C. Then, washing was performed as previously described and PI was added in the last washing solution before *in situ* observation under confocal microscope. The quantity of bacteria was determined on the double-channel RGB images using ImageJ® 1.47V software. Bacteria with active green GFP metabolism or damaged membrane as demonstrated by PI staining are called “Live” and “Damaged” in the following text, respectively. For each experiment, 7 locations were observed on each surface sample, and two identical substrates of each type were analyzed. Experiments were repeated three times. Results are expressed as average ± standard deviation. Significance of differences was tested by Student *t*-test.

3. RESULTS

3.1. TiO_2 and polyelectrolyte film construction monitoring and characterization

First, X-Ray Diffraction analysis showed that the procedure applied to the Aeroxide® TiO_2 P25 suspension with final centrifugation step removed some larger size TiO_2 crystallites from the TiO_2 suspension (Figure S1A, Table 1). Indeed, the suspension used for LbL was found to be composed of 92 wt.% anatase with mean crystallite sizes of 17 nm for anatase, and 22 nm for rutile, while a slightly higher fraction of rutile phase was observed at 19% for the P25 TiO_2 powder, with slightly higher mean crystallite sizes of 20 and 32 nm, respectively, for anatase and rutile phases.

Considering analysis accuracy, the XRD patterns recorded for single layer pair and 10 layer pairs LbL films constructed on silicon wafers showed no preferential deposition of anatase or rutile phase (Figure S1B, Table 1). The rutile intensity peak was found to be almost in the signal threshold most likely due to the low titania content in the single layer pair film, and only the anatase phase with 18 nm in mean diameter size was observed. By contrast, the 10 layer pairs film was made of 94% anatase (18 nm) and 6% rutile (22 nm).

Dynamic Light Scattering (DLS) analyses revealed the presence of TiO_2 crystallite aggregates with a mean diameter size of 91 ± 1 nm (Figure S2), with no significant change over the time necessary for building the TiO_2/polyelectrolyte multilayer films. It is worth noting that the size homogeneity for both the individual titania crystallites and their aggregates is of importance for building homogeneous films though the layer-by-layer deposition method.

Table 1: Weight fraction and mean crystallite size of anatase and rutile phases in TiO_2 P25 as powder and from the LbL suspension, as well as in the PEI/PSS/TiO_2 film with 1 and 10 layer pairs. (*) peak intensity is too low for accurate measurements.

TiO_2 samples	**Weight fraction (wt.%) [a]**		**Crystallite size (nm) [b]**	
	Anatase	**Rutile**	**Anatase**	**Rutile**
P25 powder	81	19	20	32
P25 suspension for LbL	92	8	17	22
PEI/PSS/TiO_2	100	(*)	18	(*)
PEI/(PSS/TiO_2)$_{10}$	94	6	18	22

[a] The phase composition corresponds to the weight fraction within the crystallized TiO_2 phases determined using the most intense peaks at 25.3° and 27.1° corresponding to the diffraction of the (101) and (110) planes of anatase (JCPDS card 21-1272) and rutile (JCPDS card 21-1276), respectively. TiO_2 samples contain as well 7% of amorphous TiO_2 as determined by using the method developed in ref [51].

[b] The mean TiO_2 crystallite size, that is the average size of the coherently-diffracting domains, was determined from the Scherrer equation applied with the usual assumption of spherical crystallites to the (101) and (110) peaks of anatase and rutile, respectively.

Build-up of the PEI/(PSS/TiO_2)$_n$ films on the silicon wafer substrate (36 cm^2, 4.5 x 8 cm) was conducted by an automated dipping robot. The colors observed at the surface of the samples, arising from optical interferences, showed that titania was homogeneously deposited on the substrate (Figure 1A). The Layer-by-Layer construction of the TiO_2 and polyelectrolyte films was monitored through ellipsometry, SEM UV-visible spectrophotometry in transmission and QCM-D measurements. The ellipsometry characterization revealed the linear increase in the film thickness after the deposition of each PSS/TiO_2 layer pair, with an average apparent thickness increment of 40 nm ± 5 nm per PSS/TiO_2 layer pairs as well as a good film thickness homogeneity materialized by the low standard deviations (Figure 1B, Table 2). While the average aggregate size was found to be centered at 91 ± 1 nm, the thickness of the titania layer was found to be lower than the DLS measurement, but higher than the mean crystallite size of the main phase, i.e. anatase, derived from XRD. This may indicate that the sample's surfaces are not fully homogeneously covered by 20 nm diameter anatase crystallites, but rather by small-size TiO_2 aggregates, providing an average thickness of 40 nm for the layers, and creating a high porosity within the layered films films that directly results from the inter-crystallite space as well as from the space between the TiO_2 aggregates. This might be more pronounced for the single layer pair film, for which the average thickness of the layer was higher than that calculated for the next (upper) layers.

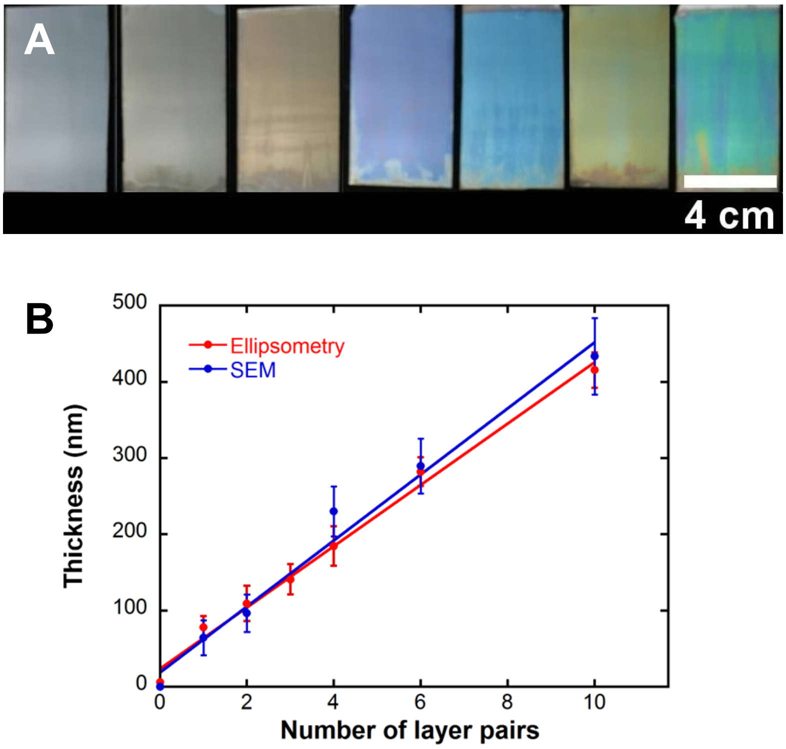

Figure 1: (A) Optical photographs of PEI/(PSS/TiO_2)$_n$ films built on silicon wafers. From left to right: bare silicon wafer, PEI/PSS film, PEI/PSS/TiO_2, PEI/(PSS/TiO_2)$_2$, PEI/(PSS/TiO_2)$_4$, PEI/(PSS/TiO_2)$_6$ and PEI/(PSS/TiO_2)$_{10}$. **(B)** Increase in thickness of PEI/(PSS/TiO_2)$_n$ LbL films obtained by ellipsometry and SEM as a function of the number of layer pairs. A linear increase in thickness is observed at the deposition conditions reported here.

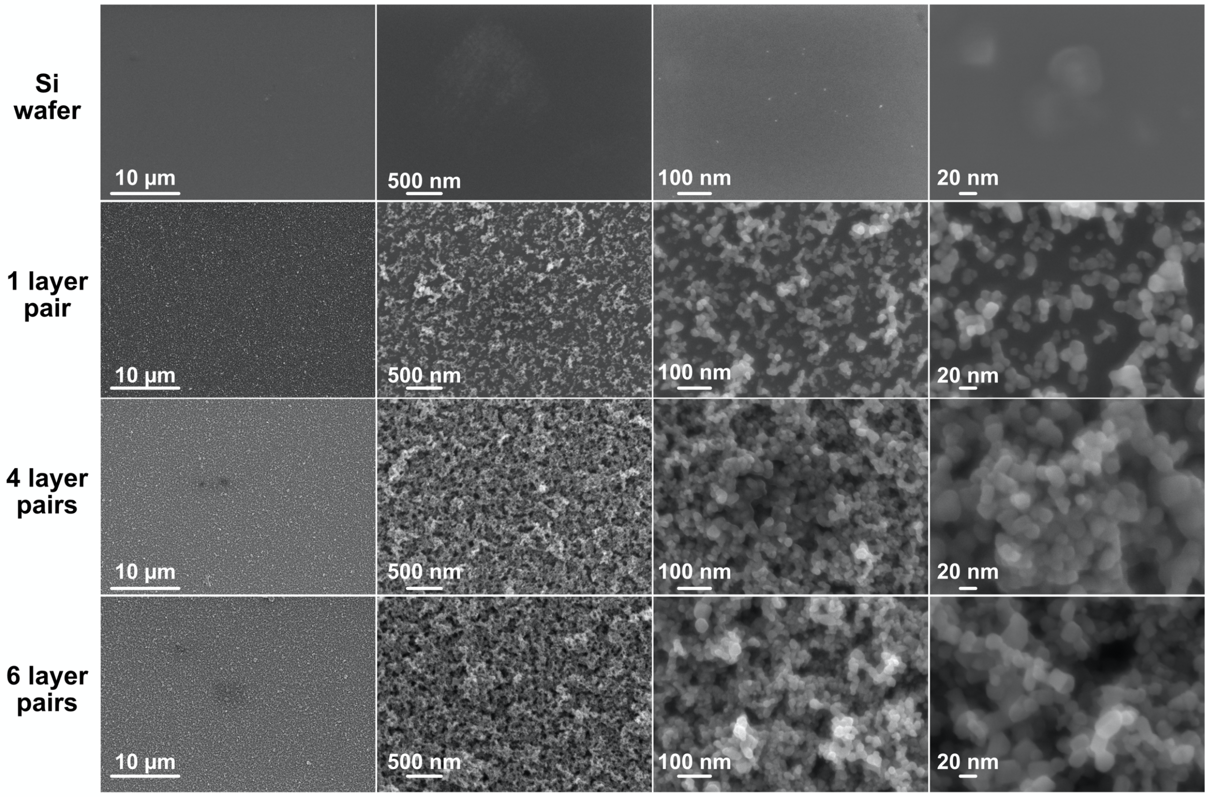

Figure 2: SEM images of titania and polyelectrolytes LbL films built on silicon wafers, with different numbers of PSS/TiO_2 layer pairs. It must be stressed that on the thicker films such as eg. the 6 layer pair film, the dark zones do not correspond to the naked substrate (ie. TiO_2-free zones), but appears dark due to a thickness contrast effect (see further the cross-section images evidencing the complete substrate coverage when increasing the number of layer pairs).

The SEM images of the PEI/(PSS/TiO_2)$_n$ films showed the homogeneity of the films at the micrometer scale, whatever the number of layer pairs, while on the contrary they clearly revealed their heterogeneity at the nanometric scale, which provides to the films their porous structure, as visualized on both top-view and cross-section images (Figures 2 and 3). This porous structure was also observed on PSS/TiO_2 LbL films on different substrates in the works of Rongé et al.[33] and Dontsova et al.[32] While a fairly good coverage of the silicon wafer by TiO_2 nanoparticles was already observed for a single layer pair film, the cross sections images did not show any stratified structure with well-defined polyelectrolyte and titania layers, and the surface coverage became total and the films became denser with the increase in the number of layer pairs (Figure 3). An average thickness increase of 43 nm per layer pair was derived from the film cross section analysis, in agreement with the ellipsometry results (Table 2 and Figure 1B).

Table 2: Film thickness obtained by ellipsometry and SEM characterisations.

Sample	**Ellipsometry (nm)** [a]	**SEM cross section (nm)** [b]
PEI/PSS/TiO_2	78 ± 15	65 ± 23
PEI/PSS/$(TiO_2)_2$	110 ± 23	97 ± 25
PEI/PSS/$(TiO_2)_3$	141 ± 20	-
PEI/PSS/$(TiO_2)_4$	185 ± 27	230 ± 33
PEI/PSS/$(TiO_2)_6$	282 ± 19	290 ± 36
PEI/PSS/$(TiO_2)_{10}$	416 ± 23	434 ± 50

[a] Whatever the number of layer pairs of the films, no significant change in the thickness of the films was observed after the gas phase photocatalytic tests under UV-A.

[b] We have to stress that the cross-sections may have slightly suffered from the heat produced by the ion beam. They however stay in good agreement with the values derived from ellipsometry.

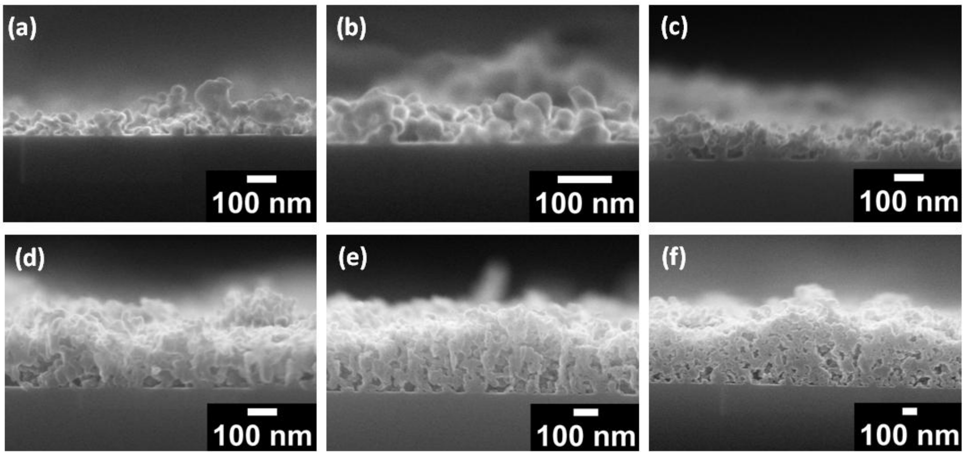

Figure 3: Cross section SEM images of PEI/(PSS/TiO_2)$_n$ LbL films built on silicon wafers. n=1 (a and b), n=2 (c), n=4 (d), n=6 (e) and n=10 (f). Brightness and contrast of SEM images were treated with Image J®.

The LbL film construction was also monitored though QCM-D experiments, that showed that no film deconstruction occurred while performing the alternate dipping and rinsing process (Figure 4 and Figure S3). Moreover, the difference in frequency changes while depositing materials has shown that the amount of PSS is increasing after every deposition step (Table S1), indicating that either more PSS is deposited after each deposition step, or more water molecules are adsorbed on the film. The superhydrophilicity of PSS/TiO_2 LbL films after 2 layer pairs have been deposited, may have played a role, as proposed by Kommireddy *et al.*[52] High dissipation values highlight the adsorption of water on LbL films after each titania nanoparticle deposition, and suggests that PSS/TiO_2 does not act as a rigid film, but more like a viscous one, as confirmed by the absence of any curve overlap for the frequency changes at the different overtones analysed.

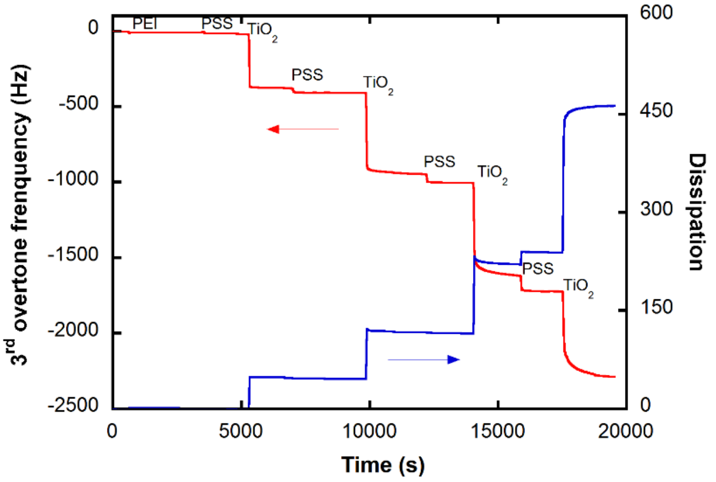

Figure 4 : Monitoring PEI/$(PSS/TiO_2)_n$ film construction by QCM-D at the 3rd overtone. 4 PSS/TiO_2 layer pairs were deposited.

The above-mentioned characterizations were also implemented for estimating the amount of titania deposited per layer. QCM-D data at the 3rd overtone (n = 3) indicated the deposition of 6.3 $\mu g/cm^2$ of TiO_2 within the first layer pair, while an average of 10.1 ± 0.7 $\mu g/cm^2$ of TiO_2 deposited was estimated for the subsequent layers (ie. excluding the first layer pair). However, this value includes the amount of water adsorbed onto the film, which increased the mass of deposited material. Therefore, while the first layer deposited is reasonable to determine the amount of material deposited, the amount of materials deposited in the films for the next layers is overestimated ; indeed, the deposition of the next layers does not include the drying step using QCM and the exact modelling of dissipation and mass appeared too complex in such a system.

The film construction was also monitored on quartz slides through UV-visible spectrophotometry in transmission mode (Figure 5). A linear increase in absorbance in the UV region was observed while depositing TiO_2 layers on the substrate surface, indicating that the multilayer building process increased regularly the amount of TiO_2 within the film. More precisely, absorbance and transmittance values at 300 nm in wavelength were recorded, in regards to the number of layer pairs deposited. This wavelength was suitable since PSS absorbs at 225 nm, which therefore does not affect absorbance results at 300 nm.[30] Results showed a linear increase of 0.28 in absorbance per layer pair, while an exponential decay profile was reported for the transmittance at 300 nm with increasing the number of layer pairs. Hence, a film composed of six layer pairs displayed a low residual transmittance of 2%.

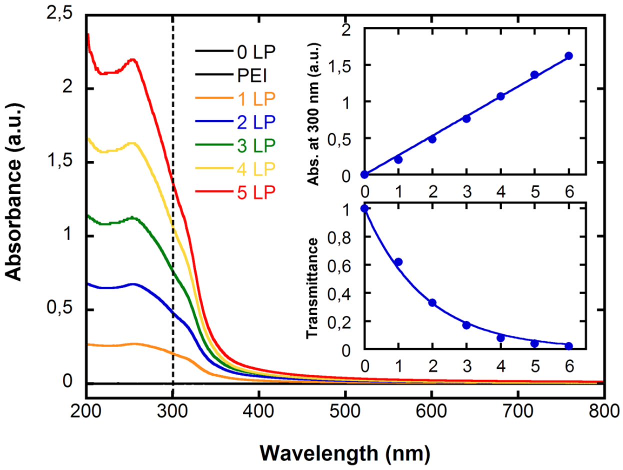

Figure 5: UV-Visible spectrophotometry characterisation in transmission mode of the PEI/(PSS/TiO_2)$_n$ films built on quartz slide, with absorbance increment after each layer pair deposited. (Insets) absorbance and transmittance at 300 nm in regards to the number of layer pairs deposited.

By neglecting the light scattering and assuming identical extinction values of TiO_2 in aqueous suspension and in the LbL titania films built on quartz slide, UV-Vis spectrophotometry in transmission mode can be considered as a valuable time-saving and cheap method for approximating the titania amount increment per layer pair. From Supporting Information SI2, it has been estimated at 4.7 ± 0.5 µg/cm².

By contrast to both QCM-D and UV-vis spectrophotometry measurements, the ICP-AES chemical analysis operates without assumptions and neglected parameters, for providing accurately the amount of titanium within the films. It evidenced a linear increase in the amount of titania deposited on silicon wafer with a density of 7.0 ± 0.7 µg/cm² per layer deposited (Figure S4), and the values derived from ICP-AES measurements were used further in the study. The fill factor *f* of the film was consequently estimated at 0.44 (Supporting Information SI3). In comparison to that of about 0.74 observed for hexagonally close-packed hard spheres, this corroborates the porous structure of the film.

Each physical measurement is limited in accuracy by the specific sample in a specific experiment and by the models applied for deriving the data, so that it is not surprising that some methods slightly differ with respect to the determination of a specific quantity. The key-aspect is that all data fall into the same ballpark, which they do in our case, and that the obtained data allows the monitoring of the multilayer films's construction.

3.2. Photocatalytic activity

Figure 6A-D depicts the influence of the number of layer pairs on the performances of the PEI/$(PSS/TiO_2)_n$ films in the degradation of the HCOOH pollutant, expressed in terms of HCOOH conversion, number of HCOOH molecules degraded per unit of time and of catalyst mass, apparent quantum yield η_{app}, quantum yield η and concentration of CO_2 formed, the values being summarized in Table 3. It shows that the HCOOH conversion profile followed an unusual behaviour with the increase in the number of layer pairs, ie. with the increase in the amount of titania within the film (Figure 6A). Indeed, for such low thickness films, ie. films in the 50-500 nm thickness sub-micronic range with low TiO_2 content, the conversion was expected to be proportional to the amount of photocatalyst.[53,54] By contrast, a high HCOOH conversion of 94% was observed for a single layer pair film, with a decrease of conversion rate for films containing a second and third layer of titania, respectively 63% and 60%. For a higher number of layer pairs, the photocatalytic conversion increased to 72% and subsequently reached a plateau after 6 layer pairs in the film, with a conversion rate of 86-88%.

After normalization to the amount of TiO_2 photocatalyst in the film, Figure 6B depicts as well the unusual behaviour of the film composed of a single layer pair, for which the highest number of HCOOH molecules degraded per unit of time and of catalyst mass (ie. in mol/µg/min) was achieved. As soon as a second layer pair was built, this number first drastically dropped down, before it further slightly decreased with increasing the number of layer pairs, evidencing that most of the HCOOH degradation is done here by the upper layers.

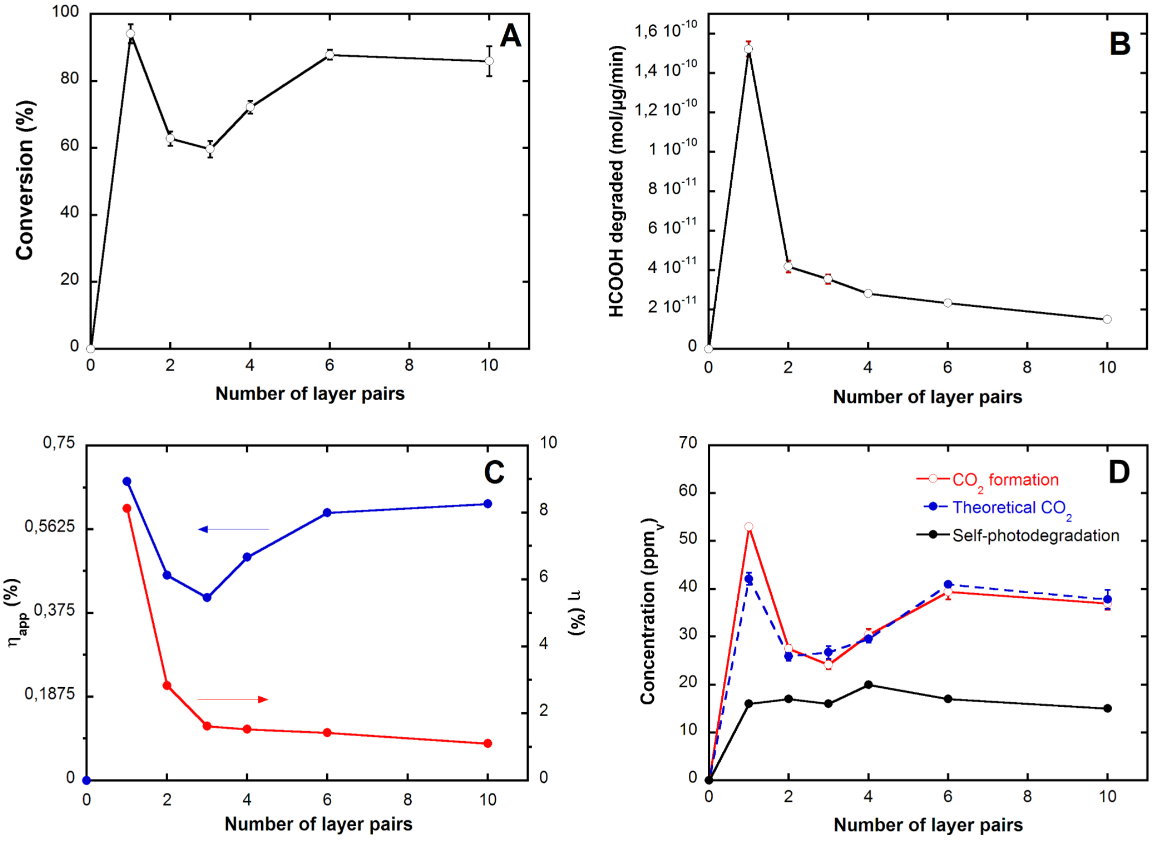

Figure 6: Influence of the number of layer pairs on **(A)** the HCOOH conversion, **(B)** the number of HCOOH molecules degraded in mol per µg of TiO_2 per minutes, **(C)** both apparent quantum yield η_{app} and quantum yield η, and **(D)** the CO_2 concentration, obtained with the LbL PEI/(PSS/TiO_2)$_n$ films. Experimental parameters: [HCOOH] = 45 ppm$_v$, air flow = 20 mL/min, speed = 0.7 cm/s, UV-A irradiance = 2.5 mW.cm^{-2}, films built on 36 cm^2 silicon wafers. On the graph (D), the concentration of CO_2 stoichiometrically formed from the converted HCOOH is reported for comparison, as well as the CO_2 concentration formed upon UV-A irradiation of the films in the absence of any inlet HCOOH flow (total humid air flow of 20 mL/min).

The CO_2 formation curve followed the same trend than that of the HCOOH conversion, with a maximum CO_2 concentration formed of 53 ppm$_v$ for a single pair of layer film (Figure 6D and Table 3). The CO_2 concentration decreased once adding a second and a third PSS/TiO_2 layer pair, to 28 and 24 ppm$_v$, respectively, before subsequently increasing and reaching a plateau at about 38 ppm$_v$ after 6 layer pairs films. As observed for the HCOOH conversion results, the CO_2 value obtained for a single layer pair film overcomes those obtained on films with a higher number of layer pairs. In comparison to the amount of CO_2 stoichiometrically formed from the converted HCOOH, an overproduction of 11 ppm$_v$ was observed for the PEI/PSS/TiO_2 LbL film. Therefore, upon irradiation, a single layer pair film PEI/PSS/TiO_2 may not only degrade gas phase formic acid, but may also degrade polyelectrolytes contained within the film. However, this overproduction was suppressed once a second layer pair was constructed, so that the LbL titania film is degrading mainly HCOOH and not the polyelectrolytes, and the CO_2 concentration formed corresponds to the stoichiometric concentration formed by the oxidation of HCOOH.

Further, independently of the number of layer pairs within the film, submitting the film to the same flow rate and light conditions but in the absence of any inlet HCOOH pollutant led to the formation of a small amount of CO_2 (ca. 16 ppm_v), close to the CO_2 overproduction obtained on the PEI/PSS/TiO_2 single layer pair film during the photocatalytic oxidation of HCOOH. The results suggest that the photocatalytic self-degradation of the PEI/(PSS/TiO_2)$_n$ LbL films upon UV-A irradiation is concerned more with the degradation of the PEI polyelectrolyte rather than with that of PSS, since the CO_2 formation remains independent of the number of PSS/TiO_2 layer pairs within the film. This did not impact on the stability of the performances, as no reduction of the photocatalytic efficiency of the films was observed when the test duration was extended over more than 24 h, as expressed in the section 2.5. In consequence, reusability tests performed on some of the films by introducing a darkness period of 12 h between two tests under illumination did not reveal any change neither in the HCOOH conversion nor in the CO_2 formation.

The photocatalytic activity of the films was also expressed in terms of apparent and efficient quantum yields (Figure 6C). We know that the number of photons entering the reactor is a parameter much simpler to measure. The apparent quantum yield being related to the reaction rate and to the photons received by the titania film, and not to the absorption of the film, the results show a similar trend to the HCOOH conversion curve with a maximum apparent quantum yield for a single layer pair film (0.67%), followed by a decrease in yield until 3 layer pairs film (0.41%). The apparent quantum yield then increases again up to a plateau level at about 0.6% for a film composed of 6 – 10 layer pairs.

As far as the quantum yield assessment was concerned by considering the light absorption profile of the films, although the reflective surfaces can lead to measurement approximation due to light back-scattering or forward-scattering from the catalyst particles,[55] a maximum quantum yield of 8.1% was obtained for a single layer film, which is 6-7 times higher than the quantum yields achieved with 6-10 LP films, at ca. 1.1-1.4%.

Table 3. HCOOH conversion, number of HCOOH molecules degraded per unit of time and of catalyst mass, apparent quantum yield η_{app}, quantum yield η, concentration of CO_2 formed and theoretical concentration of CO_2 formation, as a function of the number of layer pairs and of the TiO_2 content in the PEI/$(PSS/TiO_2)_n$ films.

Multilayer films	**Amount of TiO_2 deposited (µg/cm²) [a]**	**HCOOH conversion (%)**	**HCOOH molecules degraded ($x10^{-11}$ mol HCOOH/µg TiO_2/min)**	**Apparent quantum yield, η_{app} (%)**	**Quantum yield, η (%)**	**CO_2 formation (ppm_v)**	**Theoretical CO_2 formation (ppm_v)**
PEI/PSS	0	0	0	0	0	0	0
PEI/PSS/TiO_2	7 ± 0.7	94 ± 3	15.2 ± 0.3	0.67	8.13	53 ± 1	42 ± 1
PEI/$(PSS/TiO_2)_2$	14 ± 0.1	63 ± 2	4.2 ± 0.2	0.46	2.83	28 ± 1	26 ± 1
PEI/$(PSS/TiO_2)_3$	17 ± 0.1	60 ± 2	3.5 ± 0.1	0.41	1.62	24 ± 1	27 ± 1
PEI/$(PSS/TiO_2)_4$	24 ± 0.1	72 ± 2	2.8 ± 0.1	0.50	1.53	30 ± 1	30 ± 1
PEI/$(PSS/TiO_2)_6$	41 ± 0.2	88 ± 1	2.3 ± 0.1	0.60	1.43	39 ± 2	41 ± 1
PEI/$(PSS/TiO_2)_{10}$	71 ± 0.1	86 ± 5	1.5 ± 0.1	0.62	1.10	37 ± 1	38 ± 2

[a] Values derived from ICP-AES measurements

3.3. TRMC and EPR characterization of multilayer films

Information on the number of excess charge carriers created by the TRMC pulse (I_{max}) was provided, as well as indications on life-time of charge carriers which may undergo recombination or trapping (I_{40}/I_{max}). TRMC experiments on TiO_2 based semi-conductors are often realized directly on powders, which does not necessarily reflect how the materials will behave in film. In the present case, TRMC signals have been determined directly on the multilayer films, placed at the extremity of the microwave guide.

Figure 7 depicts the time-evolution of the TRMC signal at the nanoscale recorded for the PEI/(PSS/TiO_2)$_n$ films as well as the influence of the number of layer pairs on both I_{max} and I_{40}/I_{max} parameters. No TRMC signal was observed on the bare glass slide and the PEI/PSS film used as control samples. While the I_{max} evolution profile showed that the number of photogenerated charge carriers increases according to the number of layer pairs built, i.e. with increasing the amount of TiO_2 in the film, the most useful information was related to the absence of any significant TRMC signal for the single layer pair film, from which no I_{max} and I_{40} values could consequently be extracted. This directly resulted from the low amount of titania, and allowed us to rule out the hypothesis of the generation of an especially-high number of charge carriers in respect to the amount of TiO_2 contained in the single layer pair film. Further, no significant influence of the number of TiO_2 layers on the I_{40}/I_{max} ratio was observed, indicating that the charge carrier life-times within the titania LbL films were not depending on the number of layer pairs. It must be said that no plateau was observed for the number of charge carriers created upon laser irradiation with increasing the number of layer pairs, due to the high photon density (order of magnitude equal to 10^{23} photons·s^{-1}·cm^{-2}) in comparison to that received by the films during the photocatalytic tests performed with a 2.5 mW·cm^{-2} irradiance (i.e. corresponding to an order of magnitude equivalent to 10^{15} photon·s^{-1}·cm^{-2}).

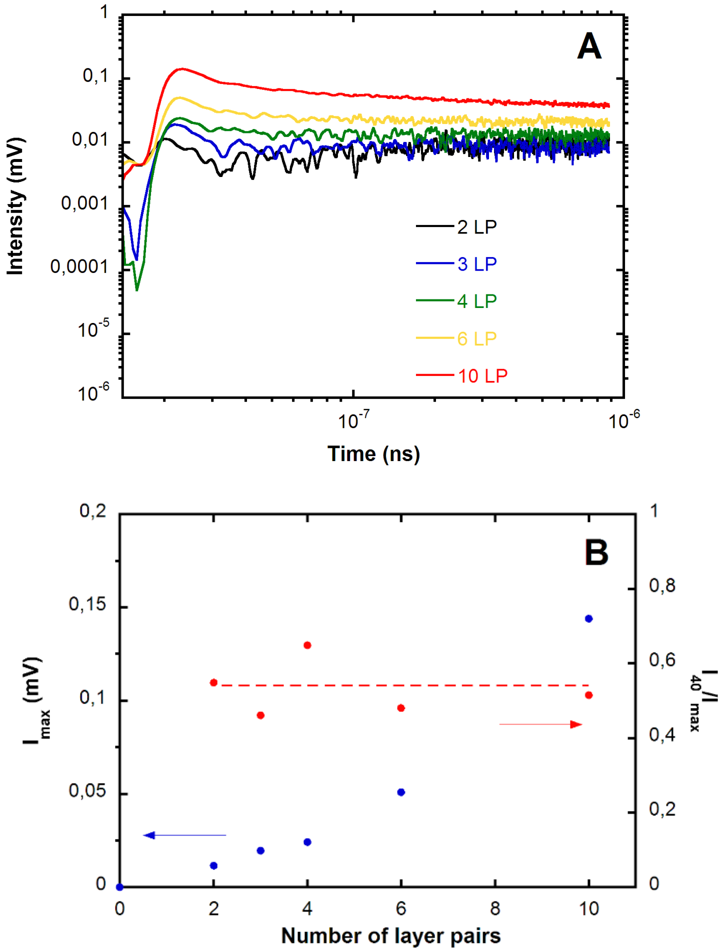

Figure 7: (A) TRMC signal obtained upon UV-A irradiation of the PEI/(PSS/TiO$_2$)$_n$ films built on glass slides. **(B)** Influence of the number of layer pairs of the LbL films on both I_{max} and I_{40}/I_{max} parameters. No significant signal could be observed for a single layer pair film, mainly due to the low amount of titania in the film, resulting in the signals being lost in TRMC threshold.

EPR characterization was performed for providing information on the electron photogeneration in the PEI/(PSS/TiO_2)$_n$ films by monitoring the TEMPOL decay signal (spin-scavenging) in regards of the UV-A illumination time.[45]. Indeed, being a stable radical, TEMPOL is reduced while reacting with photo-mediated reactive species.[56] Therefore TEMPOL decay kinetics can be directly related to the amount of accessible photogenerated electrons at the surface of TiO_2 in the film under UV-A. It must be stressed that, in contrary to the TRMC measurements, the excitation source is comparable to that used in the photocatalytic tests, i.e. neon-type with an irradiance equal to 1.5 $mW.cm^{-2}$ (which corresponds to an order of magnitude equal to 10^{15} photon s^{-1} cm^{-2}). EPR investigation of the PEI/(PSS/TiO_2)$_n$ LbL films revealed an expected trend for such films regarding the decay of the TEMPOL EPR signal, that gets faster as the number of titania layers built in the capillaries increases (Figure 8A and *k* data in Figure 8B). By normalizing the initial rate of TEMPOL reduction by the number of deposition steps (*k/n* data, Figure 8B), the average kinetic per layer pair is probed. If we first put aside the *k* and *k/n* values obtained for a single layer pair film, the decay rate *k* was proportional to the number of layer pairs, which is also expressed by almost constant *k/n* values independently of the number of layer pairs for $n \geq 3$. This evidences that the amount of photogenerated species linearly increases with increasing the number of layer pairs for $n \geq 3$, and is consequently directly proportional to the amount of TiO_2 contained in the LbL film. This indicated that no light screening phenomena was observed within the films for irradiances of an order of magnitude similar to those used in the photocatalytic tests.

By contrast, it is worth noting that the single layer pair film displayed clearly a faster decay rate of the TEMPOL EPR signal than the LbL films with 3-10 layer pairs, as the normalized *k/n* kinetics stands out of those obtained for such films (Figure 8B). This has to be put into perspective with the higher photocatalytic activity of the single layer pair film in comparison to that of thicker films.

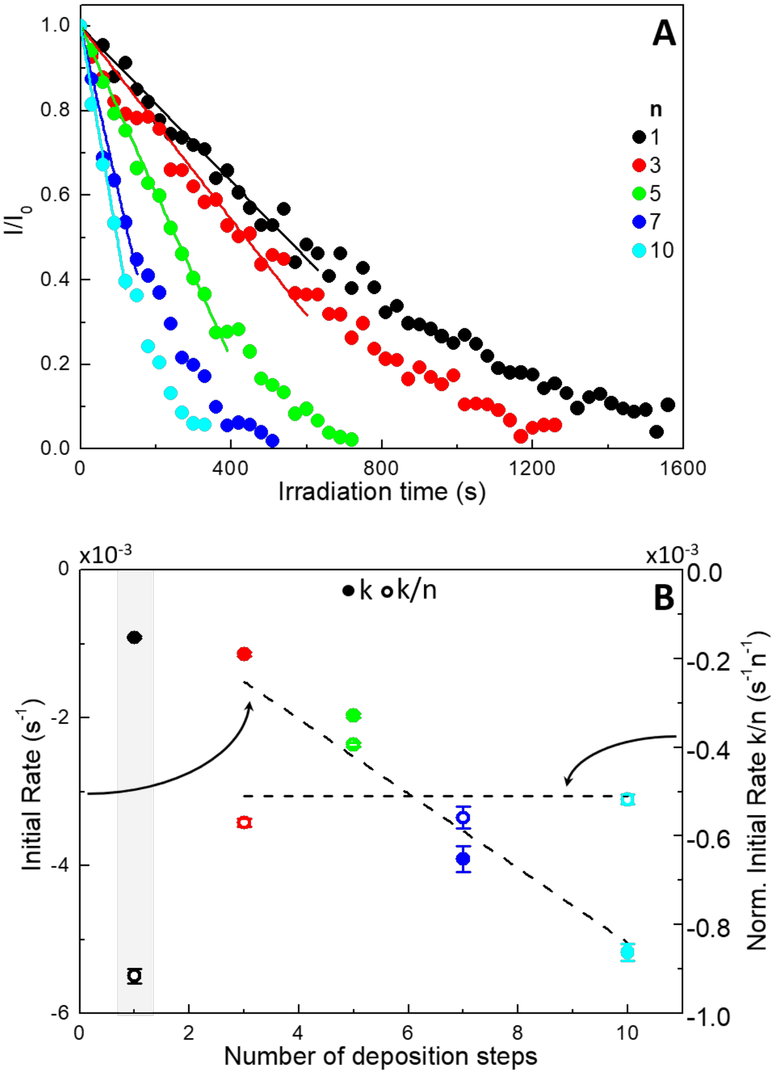

Figure 8: (A) Evolution of the normalized TEMPOL EPR intensity (I/I_0) as function of illumination time for the PEI/(PSS/TiO_2)$_n$ films with n=1, 3, 5, 7, 10, *n* being the number of deposition steps (i.e. the number of layer pairs built). **(B)** Evolution as a function of *n* of the initial rate *k* (filled circles) derived from the linear fit of the I/I_0 curve (straight lines in main graph) and of the corresponding *k/n* values normalized with the number of deposition steps. The grey area highlights the peculiar behavior obtained for a single layer pair film.

3.4. Photocatalytic antibacterial activity

The films were not sterilized prior to activity assessment for preventing them from any possible degradation of the polyelectrolytes. Unintended contamination by some microorganisms was prevented by maintaining the films in sterile milli-Q baths from their production under clean condition to their use. In addition, the titania multilayer films were shown to be stable under immersion in a NaCl aqueous solution (9 g/l) for 15 h. Indeed, ellipsometry did not reveal any decrease in film thickness, demonstrating that the films were stable in the conditions used for the bacteria assays (Table S2). On the contrary, a small increase in thickness (14 ± 7 nm) was observed, which was associated to a slight swelling of the LbL films, known to find its origin in the need of the "waterborne species" to establish an equilibrium between the solid-like film and the adjacent liquid or humidity, by regulating differences in the chemical potential or the osmotic pressure.[12]

The number of active ("Live") and damaged bacteria ("Damaged") was assessed before and after UV-A irradiation on a series of control (i.e. without TiO_2) and TiO_2-containing LbL films. Knowing ionic strength of the culture medium (Is = 0.15 M), their potential difference in surface charge especially due to the presence of TiO_2 (measured IEP at 6.1 ± 0.2) is not expected to have influenced the surface colonization by bacteria (IEP < 7 [57,58]). No significant decrease in bacteria number was observed when submitting the series of control substrate (silicon wafer) and films (PEI, PEI/PSS, PEI/PSS/PDDA, PEI/PSS/PDDA/PSS) to UV-A light for 60 min. Therefore, bactericidal properties of the silicon wafer substrate and of the immobilized polyelectrolytes under UV-A irradiation could be ruled out (Figure S5). An increase in bacteria number was even observed on these surfaces except on the silicon wafer and PEI film surfaces, whilst low numbers of damaged bacteria were counted after irradiation. This is the result of both the bacterial growth during the irradiation time and the low, harmless irradiance (3 mW.cm^{-2}) received by bacteria on the films.

Although PEI is known for its antibacterial properties [24,59] the absence of any antibacterial activity for the surface coated only with a PEI layer – and a fortiori when the initial PEI layer is masked by additional polyelectrolyte layers –, may result from the loss in mobility of PEI chains when PEI strongly adhered to the substrate as ultra-thin layer (average thickness estimated at 11.5 Å, in Felix et al. [60] This is prone to prevent immobilized PEI to intimately interact with the bacterial cell wall to significantly degrade it, as required according to the mechanism of the bactericidal action of PEI, and to make re-dissolution of PEI impossible over the time-scale of months, preventing PEI action in solution Further, only very low amount of PEI is deposited on the substrate, estimated at 119 ng/cm^2 from QCM-D measurements using the 3rd overtone.

However, "live" bacteria number on PEI surface after UV-A irradiation did not increase as much as on the other control films. Direct contact of bacteria with the PEI layer may have indeed weakened the bacterial membranes, thus resulting in an inhibition of the bacterial growth in combination with the toxic effect of irradiation. On the bare silicon wafer also, the bacterial growth expected in 60 min is inhibited under UV-A irradiation. This slight effect of 60 min UV-A irradiation on a control surface free of photocatalyst differs from Yan's results that did not report any effect of a similar irradiation time (45 min) on a glass surface.[49] However, the high reflectivity of silicon wafer (refractive index of 6.5 at 365 nm) may have cause more diffusion of light and therefore more exposition to UV-A of bacteria on silicon wafer compared to the other substrates, leading to higher toxicity of irradiation on this surface. Both minor effects were not observed on other control surfaces when additional polyelectrolyte layers were deposited on the PEI-coated substrate.

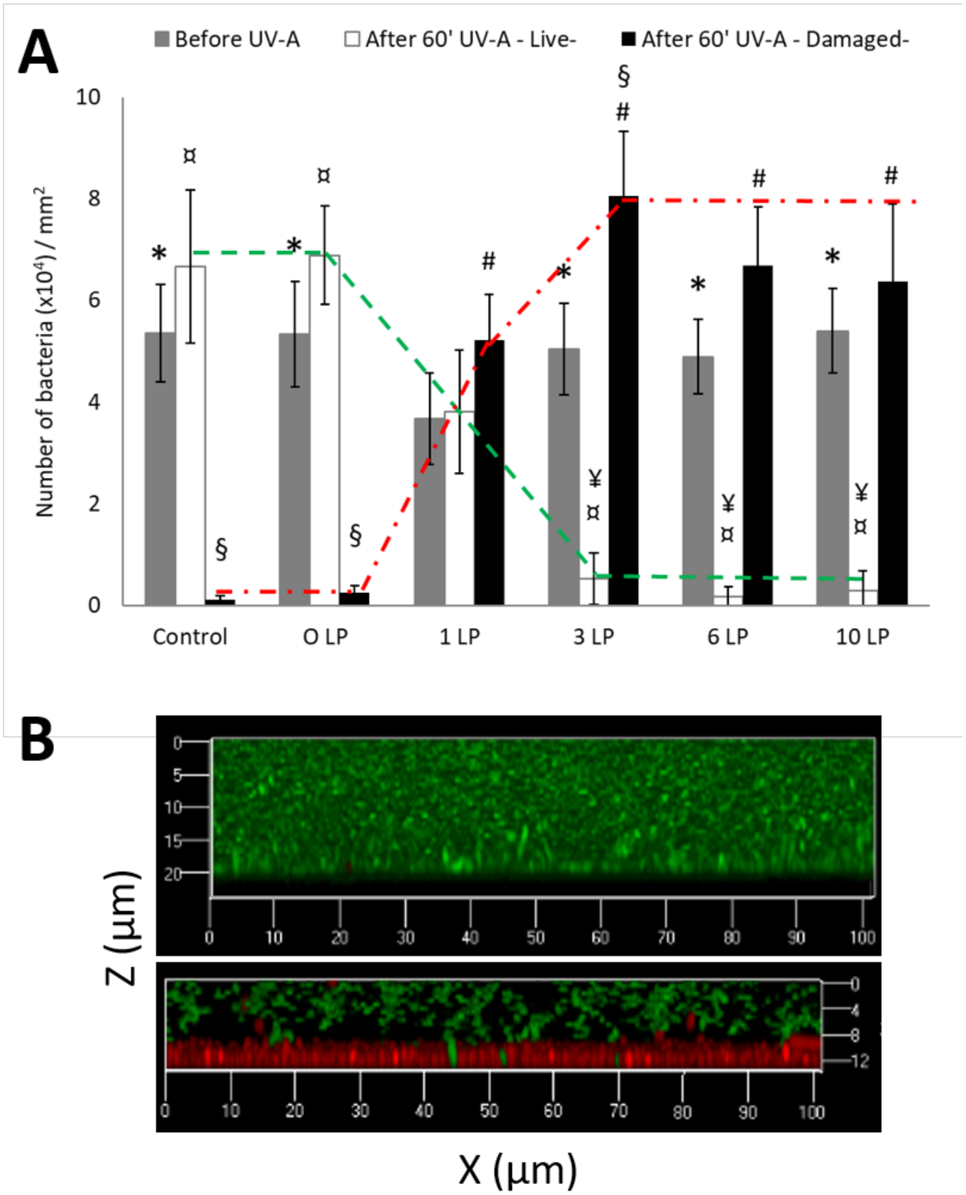

Figure 9: (A) Number of adhered *E. coli* bacteria on the control ((PEI/PSS)/(PDDA/PSS)$_9$) and the TiO_2-containing films (PEI/(PSS/TiO_2)$_n$ with n from 0 to 10), before (total population of bacteria) and after 60 min UV-A irradiation ("live" and "damaged" bacteria) (irradiance of 3 mW.cm^{-2}). Films were built on 2 cm² silicon wafers. Trends are depicted by green and red dashed

lines. *: significant difference to 1 LP before UV-A (p-value < 0.05); (¤) significant difference in live quantity compared to 1 LP after UV-A (p-value < 0.05); (¥) significant difference in live quantity compared to 0 LP, 1 LP and the control after UV-A (p-value < 0.05); (#) significant difference in damaged quantity compared to 0 LP after UV-A (p-value < 0.05); (§) significant difference in damaged quantity compared to 1 LP after UV-A (p-value < 0.05). **(B)** Cross section of biofilms visualized under confocal microscope without (top) or after (bottom) UV-A treatment and further 15 h of growth in a rich and favorable medium.

The antibacterial activity of the photocatalytic PEI/(PSS/TiO_2)$_n$ LbL films under UV-A irradiation was investigated for a number of PSS/TiO_2 layer pairs (n) varying from 0 to 10 deposited on a first PEI layer on silicon wafer (Figure 9A). The results were compared to those obtained on a control LBL film of the highest thickness i.e., with 10 layer pairs, expected to be inactive under UV-A irradiation due to the absence of TiO_2. The PEI/(PSS/TiO_2)$_n$ LbL films exhibited photocatalytic antibacterial properties upon UV-A irradiation once one single layer pair was deposited. Half of the bacteria observed on the film surface was active (“live”) whilst the other half of the population was damaged (“damaged”). Increasing the number of layer pairs from 1 to 3 caused a clear further decrease in the number of active bacteria (“ALIVE”) after irradiation with a simultaneous increase in the number of damaged bacteria (“damaged”), i.e. from 58% to 94%. Further, almost all the bacteria observed on the films were damaged after UV-A irradiation for all the films composed of more than 3 layer pairs. Bacterial cells were not completely destroyed as shown by the total population of bacteria, i.e. the sum of active and damaged bacteria, but bacteria inactivation and cell wall degradation were almost complete (from 94% to 98%) from 3 layer pairs.

The complete inactivation of bacteria adhered on TiO_2-containing coatings without complete lysis of cells is in agreement with the results reported by Yan et al. [49] for similar irradiation times. Only much longer times of photocatalytic treatment (75 h) were described to provide complete mineralization of bacterial cells adhered on TiO_2-containing surfaces, due to the high quantity of organic molecules that forms bacteria that should be degraded to completely destroy cells, as noted by other authors.[61,62] It must be noted that the reusability of the coatings depends on the cleanliness of the surface, namely the quantity of bacterial debris issued from damaged bacteria remaining on the film after use. Those debris can be eliminated by extending the photocatalytic treatment time until bacteria are completely degraded, before the newly adhered bacteria could be treated.

As a result of the high rate of bacteria inactivation, it is worth noting that the formation of biofilm after further growth in a rich and favorable medium was significantly prevented and the resulting biofilm was affected by the photocatalytic treatment as illustrated in Figure 9B. About 20% of the whole biofilm thickness (13±5 µm versus 12±4 µm after irradiation) was significantly replaced by a dense layer of damaged bacteria (0±0 µm versus 2.6±0.7 µm after irradiation) and about 50% of the analyzed sample locations revealed biofilms with sparse rather than dense active cells. In addition, a layer (2±1 µm) revealed the absence of visible active or damaged bacteria after irradiation at the bottom of the biofilm, whilst active bacteria were seen in contact with the material in the absence of treatment. This revealed the longer-term (biofilm-preventive) inactivation capacity of the photocatalytic TiO_2 films, in addition to their immediate curative photocatalytic feature.

4. DISCUSSION

4.1 Influence of the layer pair number on the multilayer films behaviour regarding formic acid mineralization

The efficiency of the films in the degradation of gaseous pollutants is considered to result from several basic features, namely (i) the TiO_2 amount in the film, here expressed in $\mu g.cm^{-2}$, (ii) the absorption of light by TiO_2 in the film, and consequently the creation of electron and hole photo-generated charges, (iii) their availability at the TiO_2 surface, that results from their transfer properties to the surface and the recombination ratio, (iv) the diffusion of the gaseous reactants within the film, and their subsequent adsorption at the surface of the irradiated TiO_2 crystallites and (v) the intrinsic surface reactivity of the TiO_2 photocatalyst.

With increasing the number of deposition steps, the construction of the films was characterized by a regular increase in the average film thickness, and was accompanied by a TiO_2 amount increment per PSS/TiO_2 layer pair deposited being independent of the layer number. The film was consequently expected to follow a usual behaviour when increasing the TiO_2 amount in the film, with a linear increase until the conversion reaches a plateau due to a screening of excess particles, which mask part of the particles due to the limited penetration thickness of UV-A light.[54,55]

Several characterization techniques were implemented on the multilayer films for assessing this light screening effect (UV-Visible spectrophotometry, EPR and TRMC measurements), for which the results might appear as contradictory at first glance. Indeed, spectrophotometry that is using a low number of incident photons (ca. 10^{11} photon s^{-1} cm^{-2}) compared to the photocatalytic test, revealed a low residual light transmission of ca. 2% for more than 6 layer pairs – that might indicate a light screening effect, i.e. fewer photons reaching the TiO_2 particles in the layers closer to the substrate. In contrast, this effect was not observed in EPR and TRMC measurements, that both confirmed that coatings with larger numbers of layer pairs produce more charges.

This apparent mismatch finds directly its origin in the irradiance level to which the films are exposed during the different characterizations, and that consequently determines the number of photons that the first exposed layer pair is receiving, and in consequence also the number of photons that the deepest TiO_2 layers are receiving. Independently of the number of incident photons, when the films are submitted to a high number of photons (*ca.* 10^{23} photon s^{-1} cm^{-2} and 10^{15} photon s^{-1} cm^{-2} in the case of TRMC and EPR characterization, respectively, the number of photons in EPR being similar to that used during the photocatalytic test, the results suggested in both cases that films with larger numbers of layer pairs – and in consequence with higher TiO_2 contents – produce more photogenerated charges. The number of the incident photons was high enough for allowing the deeper layers to still absorbed photons, and in consequence to generate charges. In that case, the PEI/$(PSS/TiO_2)_n$ films with nanometric thickness were not thick enough to suffer from any light screening effect.[63] So, one can expect that the light absorption, i.e. the number of photons absorbed by each TiO_2 layer, is in first approximation independent of the number and the location of the layer. This apparent discrepancy pointed out the necessity to apply the appropriate characterization technique in terms of light irradiance for drawing conclusions.

It must be noted that although films were built on silicon wafers, the possible reflection of the incident light by partially-covered areas of the substrate, cannot explain the high photocatalytic activity observed for the single layer film compared to that expected (extrapolated). Indeed, the number of HCOOH molecules that can be degraded could be doubled at the great maximum, while there is a factor of about 6 between both activities. In addition, the wafer coverage by a native surface oxide layer probably prevents from any charge transfer to the adjacent layer of TiO_2.

Upon UV-A light absorption, the TRMC measurements indicates that charge carriers' life time was not influenced by the number of layers in the film, so that each TiO_2 layer was considered as equivalent in terms of availability of the charges at the TiO_2 crystallite surface. In consequence, other reasons should be put forward for explaining the very high HCOOH conversion achieved on the single layer pair film with ultra-low TiO_2 content, as well as for understanding the conversion plateau observed for 6-10 layer pairs films, while no light screening was observed.

Regarding the HCOOH adsorption, no significant difference in terms of HCOOH uptake was observed in the dark between the different LbL-films before switching on the light. The first step of the HCOOH degradation, namely the adsorption at the TiO_2 surface, is reported to occur molecularly as well as dissociatively, forming unsymmetrical and bidentate formates.[64,65,66] Further, Liao et al. demonstrated that molecularly-adsorbed HCOOH has a much higher photo-oxidation rate than its dissociatively-adsorbed counterpart, as formate, and they estimated this superiority at roughly 53 times (±15% relative error) for a same surface concentration.[64] The highest rate through the direct oxidation of molecular HCOOH can be put in perspective of the two-active-sites model developed by Muggli and Backes, that computed activities differing by a factor of at least 20.[37] The conversion obtained with the films is thus mainly driven by the reactivity of the molecularly-adsorbed HCOOH reactant, since the dissociated formate is subjected to far lower photooxidation rates. Besides, regardless of the mechanism and the associated adsorption step, Liao et al. showed that the presence of co-adsorbed H_2O enhanced the oxidation rates by almost a factor 2.

If the activity obtained for a single layer pair is put aside, the increase in HCOOH conversion and in apparent quantum yield with increasing the number of layer pair clearly relates with the increase in the amount of irradiated TiO_2 crystallites in the film. The plateau of performance obtained for films built with more than 6 layer pairs was proposed to result from diffusional limitation effects within the layered $PEI/(PSS/TiO_2)_n$ film.

Indeed, keeping in mind that the photocatalytic activity of TiO_2-polymer films was reported to be influenced by the conformation of the polyelectrolytes – polyelectrolytes with extended structures enabling lower photocatalytic activity than in the case of fuzzy structures by impacting on the diffusion of organic molecules[67] –, we proposed that the diffusion of the HCOOH reactant and of the water molecules within the film might be unfavoured in too thick (dense) layered films containing charged polyelectrolytes. The hindering of the transport of HCOOH and water molecules, their co-adsorption being known to be strongly beneficial to the HCOOH conversion, would favour an efficient use of the TiO_2 upper layers. Unfortunately the transport properties of such molecules in multilayer films do not follow simple rules and the observed phenomena depend on the chemical nature of the polyelectrolytes and the chemical nature of the molecule, although the pores of the multilayer films are large enough to accommodate them.[68] The increase in the film density with the increase in the number of layer pairs was observed by SEM. This can also be put into perspective with Rongé et al., who correlated a decrease in the apparent kinetic rate constant for methylene blue degradation when increasing the layer pair deposition time, to the construction of denser TiO_2/polyelectrolyte films.[33] Upon the addition of layers, the film structure was reported to be self-organized and to become more compact, with a reduction of the film's porosity.

In addition, even though we cannot rule out that the diffusion of negatively-charged formate species in the film might be favoured in comparison to that of HCOOH, due to the existence of electrostatic interaction and local electric fields between/within the charged layers, the conversion of formate species adsorbed in the deepest layers would suffer from a very low oxidation rate, and thus would not contribute significantly to the conversion obtained on the films.

Taking those hypotheses into consideration, the high conversion and quantum yields obtained for the single layer pair film might be explained by the full availability of the titania crystallites towards both HCOOH and water molecules. This higher accessibility was also effective in the case of the TEMPOL probe molecule, and is in agreement with the highest normalized *k/n* kinetic decay rate of EPR signal in comparison to that obtained for thicker multilayer films. Consequently, the single layer pair film can take full advantage of the high photo-oxidation rate of molecularly-adsorbed HCOOH in the presence of co-adsorbed water molecules.

4.2 Photocatalytic behaviour of multilayer films with specific architectures

Specific architectures were built for testing the proposed explanation, and their efficiency was compared to that achieved on the PEI/(PSS/TiO_2) reference film with one single layer pair (Table S3). First, building $(PSS/PDDA)_8$ layers on the top of the first PSS/TiO_2 layer pair led to drastic drop of the conversion from 94% to 19%, indicating that the $(PSS/PDDA)_8$ polyelectrolyte add-layers (with a 20 nm average thickness determined by ellipsometry) are acting as a diffusion barrier for the reactants in the films. Thus, the conversion was strongly lowered compared to the reference film free of any polyelectrolyte add-layer. The low conversion of 32% and 27% obtained on the PEI/PSS/TiO_2/$(PSS/PDDA)_8$/PSS/TiO_2 and the PEI/$(PSS/PDDA)_8$/PSS/TiO_2 films, respectively, confirmed that the availability of the PSS/TiO_2 layer against the reactant remained the key-feature of the films driving the HCOOH conversion. Indeed, a direct experimental evidence for the vertical diffusion and exchange processes of polyanions and polycations in polyelectrolyte multilayer films was reported by Lavalle et al. with the possibility for the polyelectrolyte to diffuse “in” and “out” of the entire film during each bilayer deposition,[69] in agreement with theoretical works.[70] Further, Kolasinska et al. showed that charged iron oxide nanoparticles deposited on PDDA/PSS multilayer films were subjected to diffusion inside the polyelectrolyte multilayer film and were incorporated consequently into the polyelectrolyte multilayer as an interfacial “mixture” of polyelectrolyte and nanoparticles, rather than to form a 2D layer on the top of it.[71] By analogy, the building of a PSS/TiO_2 layer pair on the top of (PSS/PDDA)$_8$ layers might similarly lead to the diffusion and the (partial) incorporation of the TiO_2 nanoparticles inside the polyelectrolyte layer pairs rather than to the formation of an add-layer on the underlying (PSS/PDDA)$_8$ layers. This is consistent with the lower conversions of 32% and 27% obtained with PEI/PSS/TiO_2/(PSS/PDDA)$_8$/PSS/TiO_2 and PEI/(PSS/PDDA)$_8$/PSS/TiO_2 films, respectively, for which the polyelectrolyte layers were acting as diffusion barrier for the reactant and were lowering the availability of the incorporated TiO_2 nanoparticles. Those films, however, outperformed the PEI/PSS/TiO_2/(PSS/PDDA)$_8$ film, since the TiO_2 nanoparticles incorporated within the (PSS/PDDA)$_8$ multilayers remained probably more available for the reactant than when the (PSS/PDDA)$_8$ multilayers are directly built on the top of the PEI/(PSS/TiO_2) reference film with one single layer pair.

4.3 Antibacterial behaviour of the multilayer films *vs.* HCOOH mineralization

The increase in the antibacterial efficacy by increasing the number of layer pairs from 1 (58%) to 3 (94%) suggests that TiO_2 nanoparticles not only from the top layer pair but also from deeper layer pairs are responsible for the antibacterial activity. However, given the constant efficacy of films with from 3 to 10 layer pairs, we proposed that only the three first top layer pairs contribute to the antibacterial activity. This probably results from the impossibility for bacteria to have contact points with layers located deeper than the three first top layer pairs due to a film porosity that not matches with the micron size of bacteria. Although it is obvious that the level of photocatalytic activity of the films on a small molecule such as HCOOH and on a complex assemblage of many macromolecules such as bacterial cells should not be expected to be similar, some characteristics of the films may have especially impacted their interface to the systems to be degraded, and therefore impacted some specific performances.

Hence, the observed difference in the film behaviour against HCOOH and *E. coli* bacteria with increasing the number of layer pairs resulted

(i) from the film's surface heterogeneity at the nanometer scale, that probably enables bacteria to have contact points with TiO_2 nanoparticles located not only in the top layer but also in the underlying layers. It has been reported that increase in the number of contact points, which can be obtained via the tuning of the surface topography of the films, promotes the antibacterial efficiency of TiO_2 coatings.[49]

(ii) as well as from the porosity of the film that is in accordance with the size of a single molecule but not with the micron size of the *E. coli* bacteria, thus preventing them to diffuse within the film structure.

As a result, we proposed that the film structure allows the number of active contact points with bacteria to be increased by enabling the three first top layer pairs - but no supplementary layer pairs - to contribute to the antibacterial activity, as a result from the impossibility for bacteria to have contact points with layers located deeper due to a film porosity that not matches with the micron size of bacteria.

5. CONCLUSION

Virtually transparent TiO_2/polyelectrolyte thin multilayer films were built on model surfaces using electrostatic layer-by-layer assembly. Under UV-A irradiation such films showed excellent photocatalytic behavior for the removal of gaseous pollutant, taking HCOOH as model compound with high applicative interest, and as antibacterial surfaces, taking *E.coli* as model bacteria. Layer-by-Layer assembled PEI(PSS/TiO_2)$_n$ nano-composite coatings were prepared by immersion of different substrates in solutions containing negatively-charged NaPSS and positively-charged TiO_2 nanoparticles. The gas-phase catalytic study revealed a peculiar dependence of the photocatalytic behavior of the PEI/(PSS/TiO_2)$_n$ films as a function of the number of layer pairs, deviating strongly from the activity profile usually reported in photocatalysis. Although no light screening was evidenced, a performance plateau was observed upon an increase in the number of layer pairs ($n>6$), and was preliminarily attributed as to result from diffusion phenomena within the films that originate from the interaction of HCOOH and water with the nanoparticle/polyelectrolyte network. Most notably, a single layer pair film with a low TiO_2 content of 7 $\mu g.cm^{-2}$ outperformed films with a higher number of layer pairs, with a high quantum yield of 8.1% being 6-7 times higher than that of thicker films with higher amounts of TiO_2. The optimum accessibility of the TiO_2 crystallites in the first layer pair toward both HCOOH and water is considered to cause this unusual enhancement. In addition, we demonstrated that the three top layer pairs were contributing to the antibacterial photocatalytic activity of the PEI/(PSS/TiO_2)$_n$ films, due to the micron size of the *E. coli* bacteria as well as to the film surface heterogeneity, that allows the number of active contact points to be increased.

ASSOCIATED CONTENT

SI1 Substrate preparation

SI2 Quartz Crystal Microbalance with Dissipation monitoring (QCM-D) measurement

SI3 UV-Visible spectrophotometry in transmission mode

SI4 Time Resolved Microwave Conductivity (TRMC)

SI5 EPR characterization of multilayer films

SI6 Schematic single-pass photocatalytic reactor used for the gas phase photocatalytic tests

Figure S1 XRD characterization of Aeroxide TiO_2 P25 suspensions and of multilayer films

Figure S2 DLS characterization of the Aeroxide TiO_2 P25 suspension used for the LbL film construction

Figure S3 QCM-D measurements

Figure S4 ICP-AES chemical analysis of the multilayer films

Figure S5 Stability of films during the test protocols used for bacterial assays and control sample results

Table S1 Amount of deposited materials on LbL film calculated with QCM-D data from the 3rd overtone.

Table S2 Evolution of the multilayer film thickness after being immerged in a 9 g/l NaCl solution, obtained by ellipsometry.

Table S3 HCOOH conversion obtained on specific architectures of films in comparison to that achieved on the PEI/(PSS/TiO_2) reference film with one single layer pair.

AUTHOR INFORMATION

Corresponding Author

* nkeller@unistra.fr

Author Contributions

The manuscript was written through contributions of all authors. All authors have given approval to the final version of the manuscript. Marvin Motay elaborated all films synthesized and carried out most of the tests. Charline Soraru contributed to the microbiological studies.

Funding Sources

Funding from CARNOT MICA under the PLASMOTEX project.

ACKNOWLEDGMENT

This work is part of the PLASMOTEX project funded by the CARNOT MICA (Materials Institute Carnot Alsace). A. Rach and M. Wolf (ICPEES) are thanked for their contributions on the photocatalytic test setup. F. Courtier and M. Basler (ICS) are both acknowledged for the implementation of the illumination chamber for EPR characterization of the films.

REFERENCES

---

[1] Teoh, W.Y.; Amal, R.; Scott, J. Progress in Heterogenous Photocatalysis: From Classical Radical Chemistry to Engineering Nanomaterials and Solar Reactors. *J. Phys. Chem. Lett.* 2012, *3*, 629–639.

[2] Dionysiou, D. D.; Li Puma, G.; Ye, J.; Schneider, J.; Bahnemann D. (Eds.), Photocatalysis: Applications, RSC Energy & Environment Series N°15, The Royal Society of Chemistry, Cambridge, UK, 2016, 436 p.

[3] Ohtani, B. Photocatalysis A to Z : What We Know and What We Do Not Know in a Scientific Sense. *J. Photochem. Photobiol. C: Photochem. Rev.* 2010, *11(4)*, 157-178.

[4] Agrios, A. G.; Pichat, P. State of the Art and Perspectives on Materials and Applications of Photocatalysis over TiO_2. *J. Appl. Electrochem.* 2005, *35*, 655-663.

[5] Herrmann, J.-M. Titania-Based True Heterogeneous Photocatalysis. *Environ. Sci. Pollut. Res.* 2012, *19(9)*, 3655-3665.

[6] Dionysiou, D. D.; Li Puma, G.; Ye, J.; Schneider, J.; Bahnemann D., Eds.; *Photocatalysis: Fundamentals and Perspectives*, RSC Energy & Environment Series N°14, The Royal Society of Chemistry, Cambridge, UK, 2016, 380 p.

---

[7] Robert, D.; Keller, V.; Keller, N. Immobilization of a Semiconductor Photocatalyst on Solid Supports: Methods, Materials, and Applications, In *Photocatalysis and Water Purification: From Fundamentals to Recent Applications*, Pichat, P., Ed., Wiley-VCH Verlag GmbH & Co. KGaA, 2013; Chapter 5, pp 145-178.

[8] Nalajala, N.; Kumar Patra, K.; Bharad, P. A.; Gopinath, C. S. Why the Thin Film Form of a Photocatalyst is Better than the Particulate Form for Direct Solar-to-Hydrogen Conversion: A Poor Man's Approach. *RSC Adv.* 2019, *9*, 6094-6100.

[9] Wang, Y.; He, Y.; Lai, Q.; Fan, M. Review of the Progress in Preparing Nano TiO_2: An Important Environmental Engineering Material. *J. Environ. Sci.* 2014, 26, 2139–2177.

[10] Biswas, A.; Bayer, I. S., Biris, A. S.; Wang, T.; Dervishi, E.; Faupel, F. Advances in Top–Down and Bottom–Up Surface Nanofabrication: Techniques, Applications & Future Prospects, *Adv. Colloid Interface Sci.*, 2012, *170(1–2)*, 2–27.

[11] Decher, G. Fuzzy Nanoassemblies: Toward Layered Polymeric Multicomposites, *Science*, 1997, *277*, no. 5330, 1232-1237.

[12] Decher, G.; Schlenoff, J. B.; Eds.; Multilayer Thin Films: Sequential Assembly of Nanocomposite Materials, 2nd edition. Wiley-VCH Verlag GmbH & Co. KGaA, 2012.

[13] Nunes, B. N.; Paula, L. F.; Costa, Í. A.; Machado, A. E. H.; Paterno, L. G.; Patrocinio, A. O. T. Layer-by-Layer Assembled Photocatalysts for Environmental Remediation and Solar Energy Conversion', *J. Photochem. Photobiol. C Photochem. Rev.* 2017, *32*, 1–20.

[14] Srivastava, S.; Kotov, N. A. Composite Layer-by-Layer (LBL) Assembly with Inorganic Nanoparticles and Nanowires, *Acc. Chem. Res.*, 2008, *41(12)*, 1831–1841.

[15] Richardson, J. J.; Bjornmalm, M.; Caruso, F. Technology-Driven Layer-by-Layer Assembly of Nanofilms, *Science*, 2015, *348*, no. 6233, aaa2491.

[16] Quinn, J. F.; Johnston, A. P. R.; Such, G. K.; Zelikin, A. N.; Caruso, F. Next Generation, Sequentially Assembled Ultrathin Films: Beyond Electrostatics. *Chem. Soc. Rev.* 2007, *36*, 707-718.

---

[17] Zhao, S.; Caruso, F.; Dähne, L.; Decher, G.; De Geest, B. G.; Fan, J.; Feliu, N. ; Gogotsi, Y.; Hammond, P. T.; Hersam, M. C.; Khademhosseini, A.; Kotov, N.; Leporatti, S.; Li, Y.; Lisdat, F.; Liz-Marzán, L. M.; Moya, S.; Mulvaney, P.; Rogach, A. L.; Roy, S.; Shchukin, D. G.; Skirtach, A. G.; Stevens, M. M.; Sukhorukov, G. B.; Weiss, P. S.; Yue, Z.; Zhu, D.; Parak, W. J. The Future of Layer-by-Layer Assembly: A Tribute to ACS Nano Associate Editor Helmuth Möhwald, *ACS Nano*, 2019, *13*, 6151−6169

[18] Ariga, K.; Ahn, E.; Park, M.; Kim, B.-S. Layer-by-Layer Assembly: Recent Progress from Layered Assemblies to Layered Nanoarchitectonics, *Chem. Asian J.* 2019, *14*, 2553 – 2566

[19] Priya, D. N.; Modak, J. M.; Raichur, A. M. LbL Fabricated Poly(Styrene Sulfonate)/TiO_2 Multilayer Thin Films for Environmental Applications. *Appl. Mater. Interfaces*, 2009, *11*, 2684-2693.

[20] Faria, A.C.R.; Vebber, M.C.; Dal'Acqua, N.; Giovanela, M.; Aguzzoli, C.; Pereira, M. B.; Machado, G.; Crespo, J. S. Characterization and Application of Self-Assembled Thin Films of Polyelectrolytes/TiO_2/CdSe for Hydrogen Production, *Int. J. Hydrogen Energy* 2017, *42*, 16568–16578.

[21] Patrocinio, A. O. T.; Paula, L. F.; Paniago, R. M. Freitag, J.; Bahnemann, D. W. Layer-by-Layer TiO_2/WO_3 Thin Films as Efficient Photocatalytic Self-Cleaning Surfaces, *ACS Appl. Mater. Interfaces* 2014, *6*, 16859–16866.

[22] Truong-Phuoc, L.; Christoforidis, K.C.; Vigneron, F.; Papaefthimiou, V.; Decher, G.; Keller, N.; Keller, V. Layer-by-Layer Photocatalytic Assembly for Solar Light-Activated Self-Decontaminating Textiles, *ACS Appl. Mater. Interfaces* 2016, *8*, 34438–34445.

[23] Chai, N. N.; Wang, H. X.; Hu, C. X.; Wang, Q.; Zhang, H. L. Well-Controlled Layer-by-Layer Assembly of Carbon Dot/CdS Heterojunctions for Efficient Visible-Light-Driven Photocatalysis, *J. Mater. Chem. A* 2015, *3*, 16613–16620.

[24] Carré, G.; Garnier, L.; Moeller-Siegert, J.; Gies, J. P.; Keller, V.; Andre, P.; Keller, N. Antibacterial Textiles Functionalized by Layer-by-Layer Assembly of Polyelectrolytes and TiO_2 Photocatalyst, *RSC Adv.* 2015, *5*, 38859–38867.

---

[25] Teh, S. J.; Lai, C. W.; Abd Hamid, S.B. Novel Layer-by-Layer Assembly of RGo-Hybridised ZnO Sandwich Thin Films for the Improvement of Photo-Catalysed Hydrogen Production, *J. Energy Chem.* 2016, *25*, 336–344.

[26] Jeon, D.; Kim, H.; Lee, C.; Han, Y.; Gu, M.; Kim, B.S.; Ryu, J. Layer-by-Layer Assembly of Polyoxometalates for Photoelectrochemical (PEC) Water Splitting: Toward Modular PEC Devices, *ACS Appl. Mater. Interfaces* 2017, 9, 40151–40161.

[27] Grandcolas, M.; Sinault, L.; Mosset, F.; Louvet, A.; Keller, N.; Keller, V. Self-Decontaminating Layer-by-Layer Functionalized Textiles Based on WO_3-Modified Titanate Nanotubes. Application to the Solar Photocatalytic Removal of Chemical Warfare Agents, *Appl. Catal. A* 2011, 391, 455–467.

[28] Carp, O.; Huisman, C. L.;, Reller, A. Photoinduced Reactivity of Titanium Dioxide, *Prog. Solid State Chem.* 2004, 32(1-2) 33–177.

[29] Shibata, T.; Sakai, N.; Fukuda, K.; Ebina, Y.; Sasaki, T. Photocatalytic Properties of Titania Nanostructured Films Fabricated from Titania Nanosheets. *Phys. Chem. Chem. Phys.* 2007, *9*, 2413-2420.

[30] Nakajima, A.; Akiyama, Y.; Yanagida, S.; Koike, T.; Isobe, T.; Kameshima, Y.; Okada, K. Preparation and Properties of Cu-Grafted Transparent TiO_2-Nanosheet Thin Films. *Mater. Lett.* 2009, *63*, 1699-1701.

[31] Liu, Z.; Zhang, X.; Nishimoto, S.; Jin, M.; Tryk, D. A.; T. Murakami, Fujishima, A. Anatase TiO_2 Nanoparticles on Rutile TiO_2 Nanorods: A Heterogeneous Nanostructure via Layer-by-Layer Assembly *Langmuir* 2007, *23*, 10916-10919.

[32] Dontsova, D.; Keller, V.; Keller, N .; Steffanut, P.; Félix, O.; Decher, G. Photocatalytically Active Polyelectrolyte/Nanoparticle Films for the Elimination of a Model Odorous Gas, *Macromol. Rapid Commun.* 2011, *32*, 1145–1149.

[33] Rongé, J.; Bets, J.; Pattanaik, S.; Bosserez, T.; Borellini, S.; Sree, S. P.; Decher, G.; Martens, J.A. Tailoring Preparation, Structure and Photocatalytic Activity of Layer-by-Layer Films for Degradation of Different Target Molecules, *Catal. Today* 2015, *246*, 28-34.

---

[34] Krogman, K. C.; Zacharia, N. S.; Grillo, D. M. ; Hammond, P. T. Photocatalytic Layer-by-Layer Coatings for Degradation of Acutely Toxic Agents. *Chem. Mater.* 2008, *20*, 1924-1930.

[35] Ohno, T.; Sarukawa, K.; Tokieda, K.; Matsumura, M. Morphology of a TiO_2 Photocatalyst (Degussa, P-25) Consisting of Anatase and Rutile Crystalline Phases, *J. Catal.* 2001, *203*, 82–86.

[36] Ohtani, B.; Prieto-Mahaney, O. O.; Li, D.; Abe, R. What is Degussa (Evonik) P25? Crystalline Composition Analysis, Reconstruction from Isolated Pure Particles and Photocatalytic Activity Test, *Journal of Photochemistry and Photobiology A: Chemistry* 2010, *216*, 179–182.

[37] Muggli, D. S.; Backes, M. J. Two Active Sites for Photocatalytic Oxidation of Formic Acid on TiO_2: Effects of H_2O and Temperature, *J. Catal.* 2002, *209(1)*, 105-113.

[38] Nielsen, G. D.; Hansen, L. F.; Andersen, B.; Poulsen, N.; Melchior, O. Indoor Air Guideline Levels for Formic, Acetic, Propionic and Butyric Acid, *Indoor Air*, 1998, *8*, no. S5, 8–24.

[39] Tompkins, H. G.; Irene, E. A. Handbook of Ellipsometry, William Andrew Publishing, Springer-Verlag GmbH & Co. KG, 2005.

[40] Sauerbrey, G. *Z.* The Use of Quartz Oscillators for Weighing Thin Layers and for Microweighing. *Z. Phys A: Hadrons Nucl.* 1959, *155(2)*, 206–222.

[41] Tan, Y. P.; Yildiz, U. H.; Wei, W.; Waite, J. H.; Miserez, A. Layer-by-Layer Polyelectrolyte Deposition: A Mechanism for Forming Biocomposite Materials, *Biomacromolecules* 2013, *14(6)*, 1715−1726.

[42] Colbeau-Justin, C. ; Kunst, M. ; Huguenin, D. Structural Influence on Charge-Carrier Lifetimes in TiO_2 Powders Studied by Microwave Absorption *J. Mater. Sci.* 2003, *38*, 2429–2437.

[43] Kouamé, N. A.; Tahiri Alaoui, O.; Alexandre Herissan, A.; Larios, E.; Yacaman, M.-J.; Etcheberry, A.; Colbeau-Justin, C.; Remita, H. Visible Light-Induced Photocatalytic Activity of Modified Titanium(IV) Oxide With Zero-Valent Bismuth Clusters. *New J. Chem.* 2015, *39*, 2316.

[44] Sengele, A.; Robert, D.; Keller, N.; Colbeau-Justin, C.; Keller, V. Sn-Doped and Porogen-Modified TiO_2 Photocatalyst for Solar Light Elimination of Sulfure Diethyle as a Model for Chemical Warfare agent. *Appl. Catal. B: Environ.* 2019, *245*, 279–289.

---

[45] Twardoch, M.; Messai, Y.; Vileno, B.; Hoarau, Y.; Mekki, D.; Felix, O.; Turek, P.; Weiss, J.; Martel, D. Development of an Electron Paramagnetic Resonance Methodology for Studying the Photo-Generation of Reactive Species in Semiconductor Nano-Particle Assembled Films, *Mol. Phys.*, 2018, *116*, 1558-1554.

[46] Mills, A.; Hill, C.; Robertson, P. K. J. Overview of the Current ISO Tests for Photocatalytic Materials, *Journal of Photochemistry and Photobiology A: Chemistry* 2012, *237*, 7– 23.

[47] Yan, Y.; Keller, V.; Keller, N. On the Role of Bmimpf$_6$ and P/F- Containing Additives in the Sol-Gel Synthesis of TiO$_2$ Photocatalysts with Enhanced Activity in the Gas Phase Degradation of Methyl Ethyl Ketone, *Appl. Catal. B: Environ.* 2018, *234*, 56–69.

[48] De Lasa, H.; Serrano, B.; Salaices, M. The Energy Efficiency Factors in Photocatalytic Processes, In *Photocatalytic reaction engineering*, De Lasa, H.; Serrano, B.; Salaices, Eds. Springer, pp. 119–123.

[49] Yan, Y. ; Soraru, C. ; Keller, V. ; Keller, N. ; Ploux, L. Antibacterial and Biofilm-Preventive Photocatalytic Activity and Mechanisms on P/F-Modified TiO$_2$ Coatings. *ACS Appl. Bio Mater.* 2020, *3(9)*, 5687–5698.

[50] Miao, H.; Ratnasingam, S.; Pu, C. S.; Desai, M. M.; Sze, C. C. Dual Fluorescence System for Flow Cytometric Analysis of Escherichia Coli Transcriptional Response in Multi-Species Context. *Journal of Microbiological Methods* **2009,** *76* (2), 109-119.

[51] Cano-Casanova, L.; Amorós-Pérez, A.; Ouzzine, M.; Lillo-Ródenas, M. A.; Román-Martínez, M. C. One Step Hydrothermal Synthesis of TiO$_2$ with Variable HCl Concentration: Detailed Characterization and Photocatalytic Activity in Propene Oxidation, *Appl. Catal. B: Environ.* 2018, *220*, 645-653.

[52] Kommireddy, D. S.; Patel, A. A.; Shutava, T. G.; Mills, D. K.; Lvov, Y. M. Layer-by-Layer Assembly of TiO$_2$ Nanoparticles for Stable Hydrophilic Biocompatible Coatings, *J. Nanosci. Nanotechnol.* 2005, *5(7)*, 1081–1087.

[53] Jung, S.-C.; Kim, S.-J.; Imaishi, N.; Cho, Y.-I. Effect of TiO$_2$ Thin Film Thickness and Specific Surface Area by Low-Pressure Metal–Organic Chemical Vapor Deposition on Photocatalytic Activities, *Appl. Catal. B: Env.* 2005, *55(4)*, 253-257.

---

[54] Herrmann, J.-M. Photocatalysis Fundamentals Revisited to Avoid Several Misconceptions. *Appl. Catal. B: Env.* 2010, *99*, 461–468

[55] Fox, M. A.; Dulay, M. T. Heterogeneous Photocatalysis, *Chem. Rev.* 1993, *93(1)*, 341–357.

[56] Matsumoto, K.; Nagata, K.; Yamamoto, H.; Endo, K.; Anzai, K.; Aoki, I. Visualization of Free Radical Reactions in an Aqueous Sample Irradiated by 290 MeV Carbon Beam, *Magn. Reson. Med.*, 2009, *61(5)*, 1033–1039.

[57] Montag, D.; Frant, M.; Horn, H.; Liefeith, K. Dependence of theIinitial Adhesion of Biofilm Forming Pseudomonas putida mt2 on Physico-chemical Material Properties, *Biofouling*, 2012, *28 (3)*, 315-327.

[58] Sherbet, G. V.; Lakshmi, M. S. Characterisation of Escherichia coli Cell Surface by Isoelectric Equilibrium Analysis, *Biochim. Biophys. Acta*, 1973, *298(1)*, 50-58.

[59] Beyth, N.; Kesler Shvero, D.; Zaltsman, N.; Houri-Haddad, Y.; Abramovitz, I.; Davidi, M. P.; Weiss, E. I. *PLoS One* 2013, *8*, e78586.

[60] Felix, O.; Zheng, Z.; Cousin, F.; Decher, G. Are Sprayed LbL-Films Stratified? A First Assessment of the Nanostructure of Spray-Assembled Multilayers by Neutron Reflectometry, *C. R. Chimie,* 2009, *12*, 225-234.

[61] Jacoby, W. A.; Maness, P. C.; Wolfrum, E. J.; Blake, D. M.; Fennell, J. A. Mineralization of Bacterial Cell Mass an a Photocatalytic Surface in Air. *Environ. Sci. Technol.* 1998, *32(17)*, 2650-2653.

[62] Karbasi, M.; Karimzadeh, F.; Raeissi, K.; Rtimi, S.; Kiwi, J.; Giannakis, S.; Pulgarin, C. Insights Into the Photocatalytic Bacterial Inactivation by Flower-Like Bi_2WO_6 Under Solar or Visible Light, Through In Situ Monitoring and Determination of Reactive Oxygen Species (ROS). *Water* 2020, *12*, 1099.

[63] Xianyu, W. X.; Park, M. K.; Lee, W. I.; Thickness Effect in the Photocatalytic Activity of TiO_2 Thin Films Derived from Sol-Gel Process. *Korean Journal of Chemical Engineering* 2001, *18*, 903–907.

[64] Liao, L.-F.; Wu, W.-C.; Chen, C.-Y.; Lin, J.-L. Photooxidation of Formic Acid vs Formate and Ethanol vs Ethoxy on TiO_2 and Effect of Adsorbed Water on the Rates of Formate and Formic Acid Photooxidation. *J. Phys. Chem. B* 2001, *105*, 7678-7685.

---

[65] Popova, G. Y.; Andrushkevich, T. V.; Chesalov, Y. A.; Stoyanov, E. S. In Situ FTIR Study of the Adsorption of Formaldehyde, Formic Acid, and Methyl Formiate at the Surface of TiO_2 (Anatase), *Kinetics and Catalysis* 2000, *41(6)*, 805-811.

[66] Nanayakkara, C. E.; Dillon, J. K.; Grassian, V. H. Surface Adsorption and Photochemistry of Gas-Phase Formic Acid on TiO_2 Nanoparticles: The Role of Adsorbed Water in Surface Coordination, Adsorption Kinetics, and Rate of Photoproduct Formation. *J. Phys. Chem. C* 2014, *118(44)*, 25487–25495.

[67] Kim, T.-H.; Sohn, B.-H. Photocatalytic Thin Films Containing TiO_2 Nanoparticles by the Layer-by-Layer Self-Assembly Method, *Appl. Surf. Sci.* 2002, *201(1)*, 109-114.

[68] v. Klitzing, R.; Wong, J. E.; Jaeger, W.; Steitz. R. Short Range Interactions in Polyelectrolyte Multilayers. *Curr. Opin. Colloid Interface Sci.* 2004, *9*, 158–162.

[69] Lavalle, P.; Vivet, V.; Jessel, N.; Decher, G.; Voegel, J.-C.; Mesini, P. J.; Schaaf, P. Direct Evidence for Vertical Diffusion and Exchange Processes of Polyanions and Polycations in Polyelectrolyte Multilayer Films, *Macromolecules* 2004, *37(3)*, 1159-1162.

[70] Lavalle, P.; Picart, C.; Mutterer, J.; Gergely, C.; Reiss, H.; Voegel, J.-C.; Senger, B.; Schaaf, P. Modeling the Buildup of Polyelectrolyte Multilayer Films Having Exponential Growth, *The Journal of Physical Chemistry B* 2004, *108(2)*, 635-648.

[71] Kolasinska, M.; Gutberlet, T.; Krastev, R. Ordering of Fe_3O_4 Nanoparticles in Polyelectrolyte Multilayer Films, *Langmuir*, 2009, *25(17)*, 10292–10297.

Supporting information

Virtually Transparent TiO_2/Polyelectrolyte Thin Multilayer Films as High Efficiency Nanoporous Photocatalytic Coatings for Breaking Down Formic Acid and for E. Coli Removal

Marvin Motay,[a,b] *David Martel,*[b] *Bertrand Vileno,*[c] *Charline Soraru,*[d] *Lydie Ploux,*[d,e] *María Guadalupe Méndez-Medrano,*[f] *Christophe Colbeau-Justin,*[f] *Gero Decher,*[b] *Nicolas Keller*[a,*]

[a] Institut de Chimie et Procédés pour l'Energie, l'Environnement et la Santé (ICPEES), CNRS, Université de Strasbourg, 25 rue Becquerel 67087 Strasbourg, France

[b] Institut Charles Sadron (UPR 22), CNRS, Université de Strasbourg, 23 rue de Loess, 67034, Strasbourg Cedex 2, France

[c] Institut de Chimie, CNRS, Université de Strasbourg, CNRS, 1 rue Blaise Pascal 67008 Strasbourg Cedex, France

[d] Institut de Science des Matériaux de Mulhouse (IS2M, UMR7361 CNRS/Université de Haute Alsace), 15 rue Jean Starcky, 68057 Mulhouse, France

[e] Biomaterial Bioengineering (U1121 INSERM/Université de Strasbourg), 11 rue Humann, 67000 Strasbourg, France

[f] Institut de Chimie, CNRS UMR 8000, Université Paris-Saclay, 91405 Orsay, France

corresponding author: * nkeller@unistra.fr

Supporting Information

Supporting Information SI1

Substrate preparation

Silicon wafers (4.5 x 8 cm), glass (2.5 x 4.5 cm) and quartz slides (1.2 x 3.2 cm) were prepared as follows. The substrates were immersed in a 2 % v/v Hellmanex solution in distilled water and sonicated (ultrasound bath) for 15 min. The substrates were then rinsed with copious amounts of distilled water and then immersed in an ethanol-Milli Q water solution (50:50 v/v) and sonicated for 15 min. The substrates were then dried using compressed air and activated for 3 min using an oxygen plasma (Plasma Cleaner, Harick Plasma, New York, USA), with a power of 10,2 W applied to the radiofrequency coil. This process was repeated twice for quartz slides in order to activate both sides of the slides for UV-Visible spectroscopy characterisations. All substrates were used straight after plasma activation.

Gold coated quartz crystals for a quartz crystal microbalance with dissipation monitoring (QCM-D) were prepared by activating them with a UV/O_3 activator (UV/O_3 ProCleaner^{TM}, BioForce NanoSciences, Ames, USA) for 20 min. Gold coated quartz crystals were used straight after activation.

Supporting Information SI2

Quartz Crystal Microbalance with Dissipation monitoring (QCM-D) measurement.

QCM-D measurements were carried out on the LbL films in a QCM-D E4 (Q-Sense AB, Sweden) using flow modules in parallel. In situ LbL assemblies of TiO_2 nanoparticles and polyelectrolytes were done in a similar manner to those on macroscopic silicon or glass/quartz substrates except that for QCM-D, the LbL assembly was done in parallel. The polyelectrolyte solutions and the TiO_2 suspensions were injected into the cell (600 µl at a 300 µl/min flow) and the solutions/suspensions were kept onto the substrates until stabilisation (full adsorption) was obtained. The substrates were rinsed by injecting 3 times Milli-Q water or acid Milli-Q water (according to the used solution or suspension) and the deposition steps were repeated for building the LbL film.

Supporting Information SI3

UV-Visible spectrophotometry in transmission mode

UV-Visible (UV-Vis) spectroscopy provides information on the absorption properties of a sample. It is based on the intensity of a monochromatic radiation once it passes through (transmission mode) or reflects (reflection mode) from the sample, compared to the initial intensity. In liquid media, the absorbance measured by UV-Vis spectroscopy is related to the amount of molecules in the media being passed through by the light according to the Beer-Lambert Law:

$$A = \log\left(\frac{I}{I_0}\right) = \varepsilon \times l \times c \qquad (1)$$

where A is the absorbance or extinction of the molecules, c is the concentration of molecules in the media, l is the optical pathway corresponding to the cell length, ε is the extinction coefficient and I_0 and I are the intensity of the incident light and transmitted light respectively.

UV-visible spectroscopy in transmission mode was used in order to monitor the film construction on quartz slides. Here the optical pathway, l, corresponds to the thickness of the quartz slide. Since the film thicknesses are within the nanometric range, the film thickness is negligible in the optical pathway.

By neglecting the light scattering and assuming identical extinction values of TiO_2 in aqueous suspension and in LbL titania films deposited on quartz slide, the absorbance of the titania film can be correlated to the amount of titania per layer deposited using the following equation (Dontsova et al.) :

$$\overset{\text{Mass of TiO}_2\text{ per layer per surface}}{\frac{m}{S}} = \frac{\overset{[\text{TiO}_2]\text{ in suspension}}{c_1} \bullet \overset{\text{Optical length in suspension}}{l_1} \bullet \overset{\text{Abs of film @300nm}}{A}}{\underset{\text{Abs of suspension @300nm}}{A_1}} \qquad (1)$$

here the m/S ratio corresponds to the mass of catalyst deposited per layer per surface area (g/m²). A_1 is the suspension absorbance and A is the absorbance of one layer of the deposited material (all absorbance measurements were made at 300 nm, see Figure 5 in the article). c_1 is the concentration of the titania suspension (g/m³), l_1 the width of the quartz slide.

The absorbance of the TiO_2 suspension (A_l) can be calculated through the establishment of a calibration curve of the TiO_2 suspension absorbance against the TiO_2 suspension concentration (***left***). The estimated amount of titania deposited per layer, derived from ***right*** graph, was found to be 47 ± 5 mg/m^2 (4.7 ± 0.5 µg/cm^2).

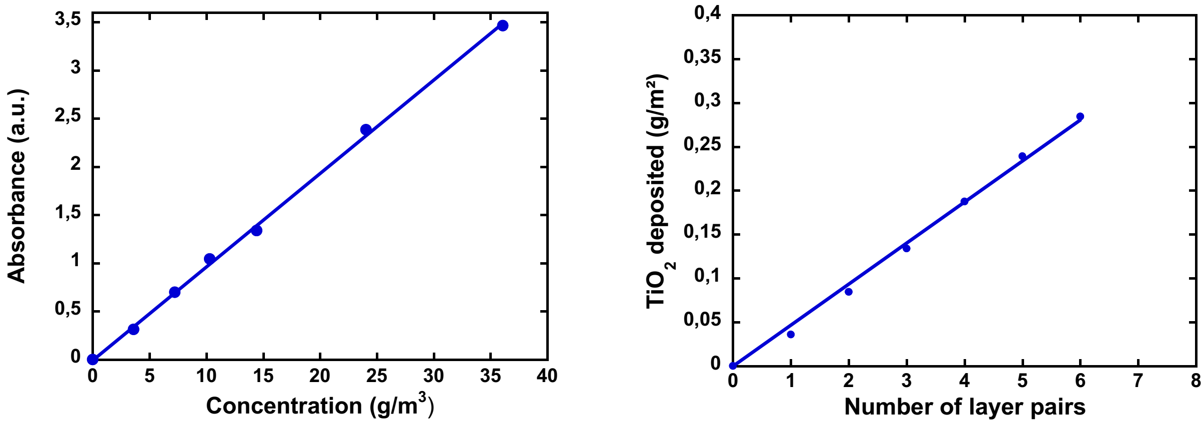

(left) Absorbance of the TiO_2 suspension in regards to the TiO_2 concentration ; **(right)** amount of TiO_2 deposited per layer pairs calculated from Dontsova's equation.

$$m = V \times d \times f \qquad (2)$$

with m the mass of TiO_2, V the volume of a monolayer with an apparent surface of 1 m^2, f the filling coefficient and d the density of TiO_2 at 4 x 10^{+6} g/m^3.

Here, with a monolayer thickness of 40 nm, the volume of a monolayer is $V = 1 \times 1 \times 40 \times 10^{-9} = 40 \times 10^{-9}$ m^3

Considering a TiO_2 amount m of 47 mg/m^2 derived from spectrophotometry (or of 70 mg/ m^2 when derived from ICP-AES, see Figure S4), the filling coefficient f was calculated as 0.29 or 0.44, respectively. This corroborated the highly porous structure of the film.

- D. Dontsova, V. Keller, N. Keller, P. Steffanut, O. Félix, G. Decher, Photocatalytically Active Polyelectrolyte/Nanoparticle Films for the Elimination of a Model Odorous Gas, Macromol. Rapid Commun., 32(15) (2011) 1145–1149.

Supporting Information SI4

Time Resolved Microwave Conductivity (TRMC)

The charge-carrier lifetimes in the LbL films upon UV illumination were determined by microwave absorption experiments using the TRMC method [1,2]. The TRMC technique is based on the measurement of the change of the microwave power reflected by a sample, $\Delta P(t)$, induced by its laser pulsed illumination. The relative difference $\Delta P(t)/P$ can be correlated, for small perturbations of conductivity, to the difference of the conductivity $\Delta\sigma(t)$ considering the following equation:

$$\frac{\Delta P(t)}{P} = A\Delta\sigma(t) = Ae\sum_i \Delta n_i(t)\mu_i \quad (1)$$

where $\Delta n_i(t)$ is the number of excess charge-carriers i at time t and μ_i their mobility. The sensitivity factor A is independent of time, but depends on different factors such as the microwave frequency or the dielectric constant. Considering that the trapped species have a small mobility, which can be neglected, Δn_i is reduced to mobile electrons in the conduction band and holes in the valence band. And in the specific case of TiO_2, the TRMC signal can be attributed to electrons because their mobility is much larger than that of the holes [3]. The incident microwaves were generated by a Gunn diode of the K_α band at 30 GHz. Pulsed light source was an OPO laser (EKSPLA, NT342B) tunable from 225 to 2000 nm. It delivers 8 ns fwmh pulses with a frequency of 10 Hz. The light energy density received by the sample was 1.3 mJ cm^{-2} at 350 nm. The main data provided by TRMC are the maximum value of the signal (I_{max}), which indicates the number of the excess charge carriers created by the pulse, including decay processes during the excitation by the laser (10 ns), and the decay ($I(t)$) due to the decrease of the excess electrons, either by recombination or by trapping processes. Concerning the decay, i.e. the lifetime of charge carriers, a short and a long range is usually analysed. The shortrange decay, arbitrarily fixed up to 40 ns after the beginning of the pulse, represented by the I_{40ns}/I_{max} ratio, reflects fast processes, mainly recombination of charge carriers, a high value indicating a low recombination speed.

1. Colbeau-Justin, C. ; Kunst, M. ; Huguenin, D. Structural influence on charge-carrier lifetimes in TiO_2 powders studied by microwave absorption *J. Mater. Sci.* 2003, *38*, 2429–2437.
2. Tahiri Alaoui, O. A. ; Herissan, C. ; Le Quoc, C. ; Zekri, M. E. M.; Sorgues, S. ; Remita, H. ; Colbeau-Justin, C. Elaboration, charge-carrier lifetimes and activity of Pd-TiO_2 photocatalysts obtained by gamma radiolysis. *J. Photochem. Photobiol. A* 2012, *242*, 34–43.
3. Fonash, S. J. Solar Cell Device Physics, Academic Press, New-York, London, 1981.

Supporting Information SI5

EPR characterization of multilayer films

LbL film construction. Capillaries were cleaned with ethanol/water (50/50 v/v) in low density sonicating bath for 15 min. They were rinsed with water and dried upon airflow. The clean substrates were first dipped 20 min in a solution of polycation PEI followed by rinsing step (dipping 3 times of 3 min in 3 different containers of ultrapure water (18MΩ.cm, Milli-Qlab system). The next steps involved alternative stages of dipping capillaries of polyanion PSS solution (20 min in HNO_3 solution adjusted pH = 2.5) and in the TiO_2 suspension adjusted by HNO3 to pH 2.5 (20 min). After each dipping steps, a rinsing step, dipping 3 times of 3 min in 3 different containers of HNO_3 solution (pH = 2.5), was performed.

Except for PEI, which was only used as first deposit, all the dipping (PSS or TiO_2) and rinsing steps were repeated to reach the desired film configuration $(PEI/PSS)/(TiO_2/PSS)_{n-1}\text{-}(TiO_2)_n$ with n = 1, 3, 5, 7, 10. Once films were constructed a final rinsing step in ultrapure water (3x5 min in 3 different containers) was performed. The last stage of the procedure was to clean the outside of the capillaries with an optical tissue soaked of ethanol in order to remove the films built.

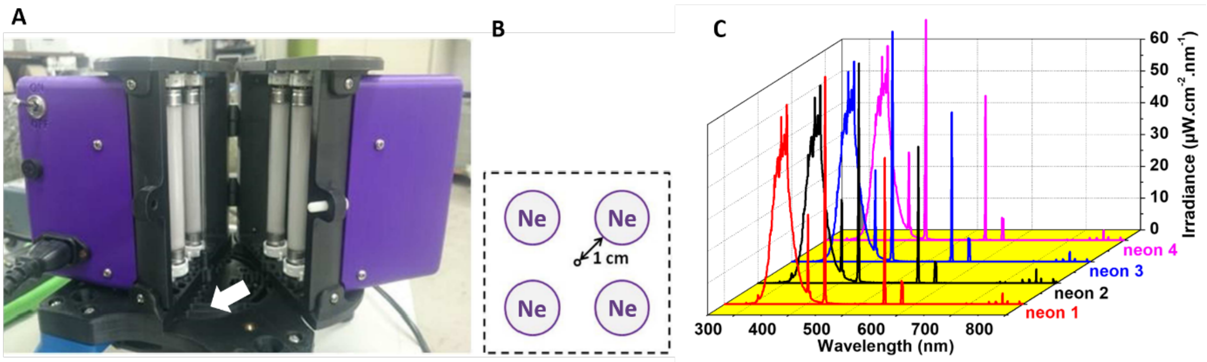

(A) Open view of the irradiation chamber equipped with a cooling fan underneath (white arrow) and composed of 4 UV-A neon tubes surrounding a clear fused quartz tube (Wilmad, 705-PQ-6.25) positioned at 1 cm of each neon allowing to centered the capillary with respect to the light source. **(B)**

schematic top view of the closed irradiation chamber. **(C)** Irradiance spectra of the 4 UV-A neon tubes used for illumination of functionalized capillaries.

Electron Paramagnetic Resonance (EPR). The coated capillaries were filled with 50 μL non-deoxygenated TEMPOL solution in water at 200 μM and sealed. A first spectrum was recorded to reach the initial EPR intensity (I_0). For all measurements, the variations of the I_0 values are less than 3%. Then, successive illumination steps of 30 s were applied. Between each illumination step, one I(t) spectrum was recorded. All the intensities values, proportional to the TEMPOL concentration ($I \propto [T\bullet]$), were obtained after baseline correction and double integrations. EPR data were plotted as I/I_0 *vs.* illumination time. Noteworthy, without the presence of paramagnetic probe, no EPR signal is detected.

Illumination of the capillaries was performed outside the EPR cavity with an UV neon-based labmade illumination chamber. Each neon presents a $\lambda_{max} = 365$ nm ($h\nu = 3.4$ eV) and $E \approx 1.5$ mW.cm^{-2} (at *ca.* 1 cm distance measured with a powermeter 1936-C and a 918D-UV-OD3 detector from Newport). The emission spectra of the neons and a schematic description of the experimental setup are depicted above. As TEMPOL does not absorb at this wavelength, there is no absorption variation during measurement. Electronic photo-generation processes occur only during the irradiation procedure and are assumed to stop as soon as light is off. All experiments were performed at room temperature (295 ± 1 K).

Supporting Information SI6

Schematic single-pass photocatalytic reactor used for the gas phase photocatalytic tests

The photocatalytic reactor was derived from that proposed in the ISO 22197 standard series. This reactor consisted of an aluminium chamber (260 mm in length x 50 mm in width x 40 mm in height) closed with a quartz window. A polytetrafluoroethylene (PTFE) support is located inside the aluminium chamber on which the pollutant flow passes. LbL films constructed on model surfaces (silicon wafers) and textiles were placed face-up in a cavity located at the centre of the PTFE support. LbL films built on 36 cm² silicon wafer were directly located in the cavity.

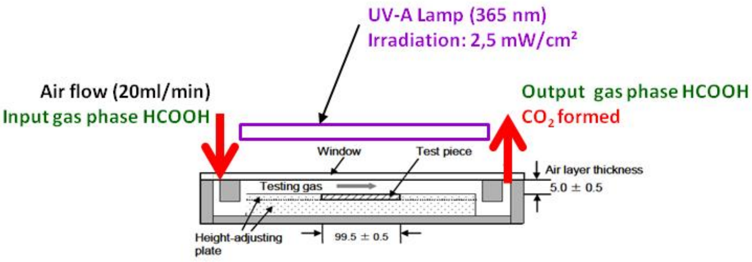

Schematic representation of the single-pass reactor containing a LbL film built on silicon wafer

A 8W UV-A lamp (Sylvania Blacklight Blue F8W/BLB T5) with a spectral peak centred at 365 nm was placed above the reactor (1.5 cm), parallel to the photocatalytic film. An irradiance of 2.5 mW/cm² was measured at the top of the sample surface. The photocalytic reactor was placed in a thermostated chamber for maintaining a constant temperature of 25°C during the test according to ISO standards, since heat generated by the lamp during the irradiation could not be neglected.

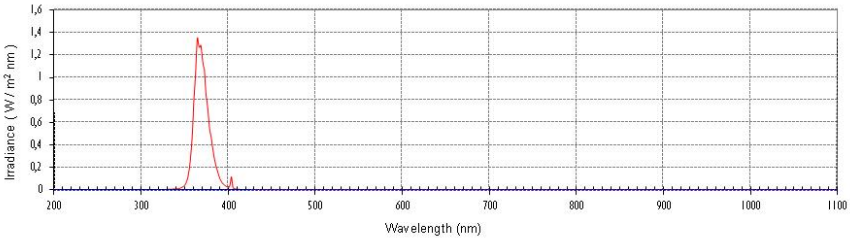

Irradiance spectrum of the UV-A lamp used in this work

The generation of the inlet polluted air flow was obtained by mixing three synthetic air flows: (i) dry air flow, (ii) humid air flow, (iii) gas-phase HCOOH containing air flow. Synthetic air was bubbled in a temperature-controlled saturator containing liquid phase formic acid (HCOOH, Sigma Aldrich, >95%) at 15°C and atmospheric pressure. Thus, the concentration of gas phase HCOOH was related to the vapour pressure of HCOOH at working temperature and pressure conditions. In the same way, synthetic air was bubbled in distilled water at 25°C and atmospheric pressure. Concentration in the gas phase was set by the vapour pressure in the working conditions. Water partial pressure was expressed in terms of relative humidity (RH): 100% of RH being defined as vapour pressure at 25°C and atmospheric pressure. These two air flows were then mixed with an additional synthetic air flow (dry air) to obtain the required pollutant-water-air ratio with a constant total air rate of 20 ml/min, corresponding to a velocity of 0.74 cm/s^{-1} and a residence time of 10.8 s in the reaction zone of the reactor. Brooks 5850 massflow meters were used to control separately dry and humid air flows. Relative humidity was set at 50% (about 3% relative to the total atmospheric pressure). In-Flow Bronkhorst flow meter (Bronkhorst® High-Tech, the Netherlands) allowed the control of HCOOH containing air flow and the photocatalytic tests were implemented at a gas phase HCOOH concentration of 45 ppm_v.

Figure S1

XRD characterization of Aeroxide TiO_2 P25 suspensions and of multilayer films

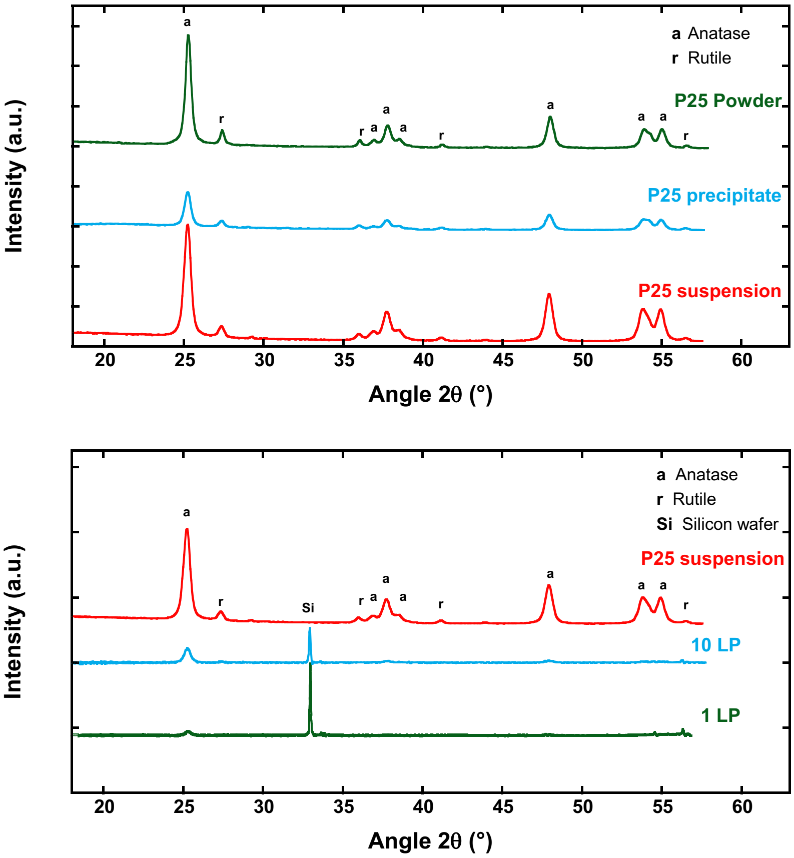

Figure S1 : XRD analysis of **(top)** TiO_2 P25 as powder and from both the precipitate and the LbL suspension, **(bottom)** the titania and polyelectrolytes LbL films with 1 and 10 layer pairs, compared to the TiO_2 P25 powder from the Lbl suspension.

Figure S2

DLS characterization of the Aeroxide TiO_2 P25 suspension used for the LbL film construction

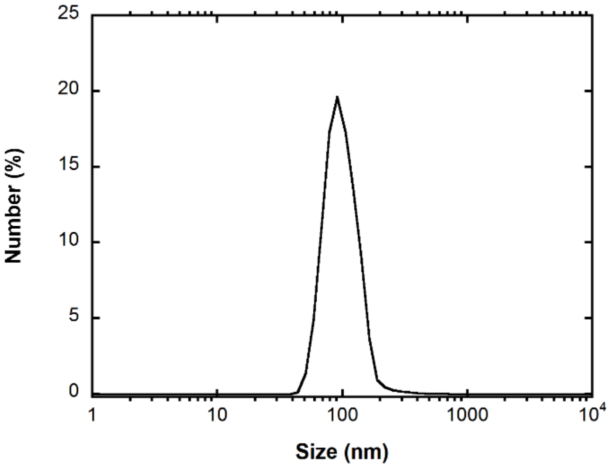

Figure S2 : Dynamic light scattering characterisation of the TiO_2 P25 suspension used for LbL film construction.

Figure S3

QCM-D measurements

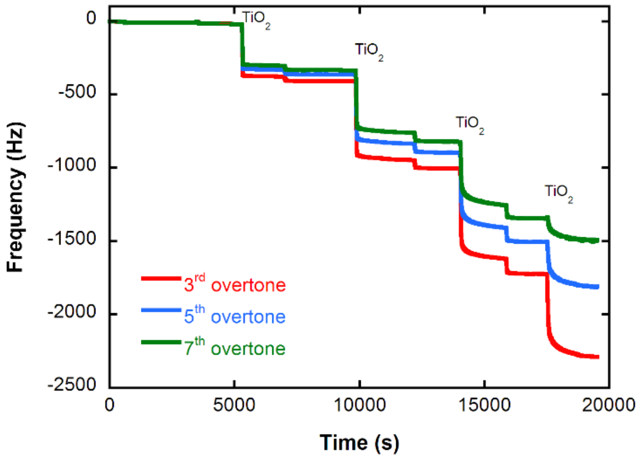

Figure S3. Change of frequency overlaying of 3rd, 5th and 7th overtones when a 4 layer pair PEI(PSS/TiO_2)$_4$ film is constructed on the QCM quartz slide.

Figure S4

ICP-AES chemical analysis of the multilayer films

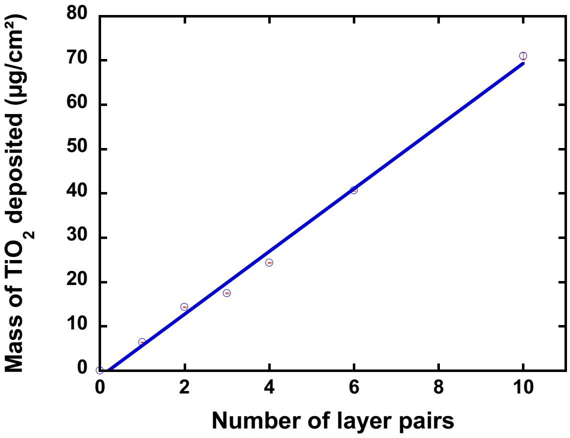

Figure S4 : Mass of TiO_2 deposited investigated by chemical analysis ICP-AES. Error bars are too small to be clearly shown on the graph.

Figure S5

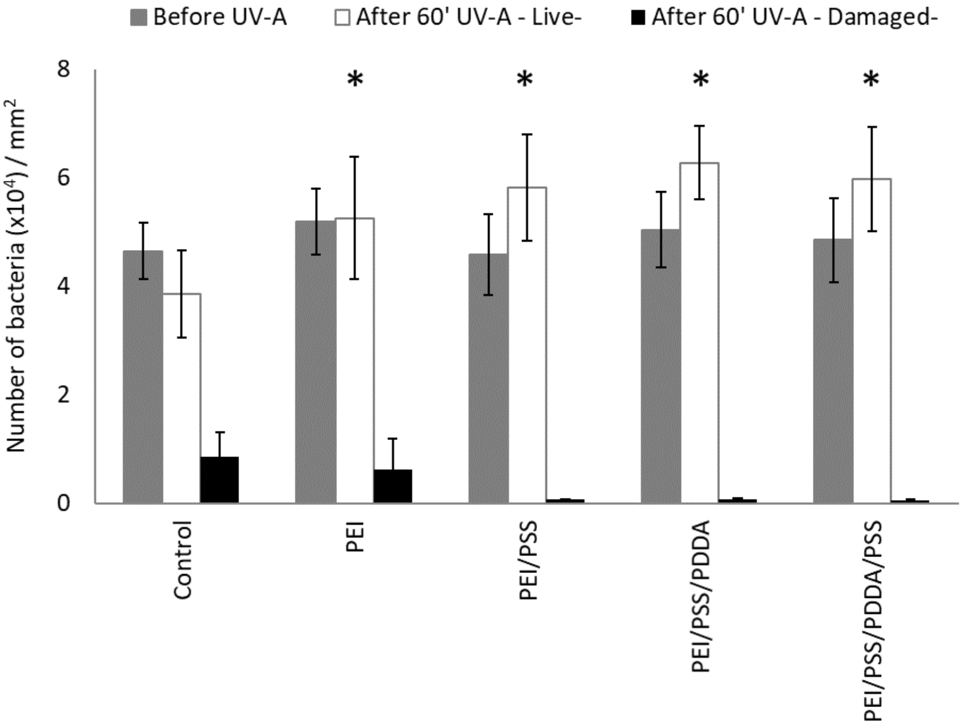

Figure S5: Number of adhered *E. coli* bacteria on control (silicon wafer) and reference films without TiO_2 (PEI, PEI/PSS, PEI/PSS/PDDA, PEI/PSS/PDDA/PSS) before (total population of bacteria) and after ("live" and "damaged" bacteria) 60 min UV-A irradiation (irradiance of 3 mW/cm². Films were built on 2 cm² silicon wafers. *: significant difference in live quantity compared to control (p-value < 0.05).

Bacterial assays were performed on control samples in order to remove any possibility of biocidal properties from the sample surface and polyelectrolyte. Reference samples were labelled as follow:

- Control: silicon wafer
- PEI
- PEI/PSS
- PEI/PSS/PDDA
- PEI/PSS/PDDA/PSS

Table S1

Layer deposited	**Mass of material deposited (ng/cm²)**
PEI	119.6
PSS #1	201.1
TiO_2 #1	6343.9
PSS #2	527.1
TiO_2 #2	9514.4
PSS #3	1024.2
TiO_2 #3	10857.8
PSS #4	1865.2
TiO_2 #4	9989.3

Table S1. Amount of deposited materials on LbL film calculated with QCM-D data from the 3rd overtone.

Table S2

Evolution of the multilayer film thickness after being immerged in a 9 g/l NaCl solution, obtained by ellipsometry

Samples	**Estimated thickness (nm)** **T = 0 h**	**Estimated thickness (nm)** **T = 15 h**
PEI/(PSS/TiO_2)$_1$	37.6 ± 2.8	47.3 ± 3.9
PEI/(PSS/TiO_2)$_4$	140.8 ± 6.2	154.6 ± 6.3
PEI/(PSS/TiO_2)$_6$	222.9 ± 8.3	246.3 ± 4.7
PEI/(PSS/TiO_2)$_{10}$	371.6 ± 9.0	380.6 ± 7.8

Table S2. Evolution of the multilayer film thickness after being immerged in a 9 g/l NaCl solution, obtained by ellipsometry. The stability of the titania LbL films for bacterial assay was assessed by being immerged in NaCl solution (9 g/l) for 15 h.

Table S3

HCOOH conversion obtained on specific architectures of films in comparison to that achieved on the PEI/(PSS/TiO_2) reference film with one single layer pair.

Table S3. HCOOH conversion obtained on specific architectures of films in comparison to that achieved on the PEI/(PSS/TiO_2) reference film with one single layer pair. Potentially active layer is visualized in italic format as *PSS/TiO_2*. Experimental parameters: [HCOOH] = 45 ppm_v, air flow = 20 mL/min, speed = 0.7 cm/s, UV-A irradiance = 2.5 $mW.cm^{-2}$, films built on 36 cm^2 Si wafers.

Film name	**Architecture specification** [a]	**HCOOH conversion (%)**
PEI/(*PSS/TiO_2*)	Reference film. TiO_2 as "final layer"	94
PEI/*PSS/TiO_2*/$(PSS/PDDA)_8$	$(PSS/PDDA)_8$ built on the top of the first PSS/TiO_2 layer pair	19
PEI/*PSS/TiO_2*/$(PSS/PDDA)_8$/*PSS/TiO_2*	$(PSS/PDDA)_8$ deposited between two PSS/TiO_2 layer pairs. TiO_2 as "final layer"	32
PEI/$(PSS/PDDA)_8$/*PSS/TiO_2*	PSS/TiO_2 layer pair built on the top of the $(PSS/PDDA)_8$ layer pairs. TiO_2 as "final layer"	27

[a] Additional $(PSS/PDDA)_8$ polyelectrolyte layer pairs were constructed using negatively-charged PSS (1 g/l at pH 2,5 adjusted by HNO_3) and positively-charged poly(diallyldimethyliammonium chloride) (PDDA, 1 g/l with 0.5M of sodium chloride) by the dipping LbL process, using the PEI/$(PSS/TiO_2)_n$ film dipping parameters. The $(PSS/PDDA)_8$ layers had an average thickness of 20 nm determined by ellipsometry.